STATISTICAL PROPERTIES OF THE LARGE SCALE STRUCTURES:

COSMIC MICROWAVE BACKGROUND ANISOTROPIES

For a review: https://www.annualreviews.org/content/journals/10.1146/annurev.astro.40.060401.093926
https://ned.ipac.caltech.edu/level5/March05/Scott/Scott_contents.html
https://arxiv.org/pdf/astro-ph/0110414.pdf

COSMIC MICROWAVE BACKGROUND RADIATION

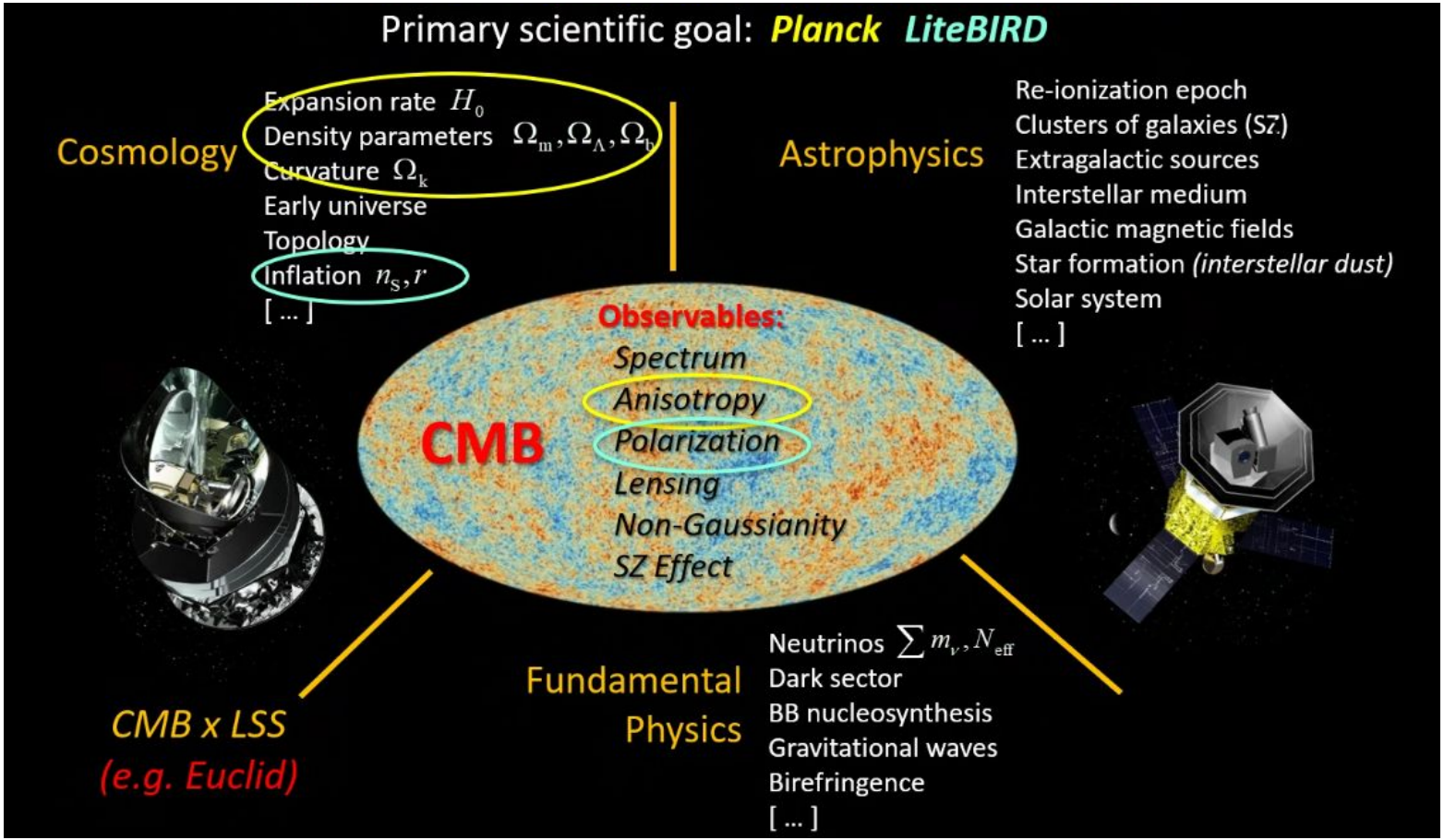

COSMIC MICROWAVE BACKGROUND RADIATION

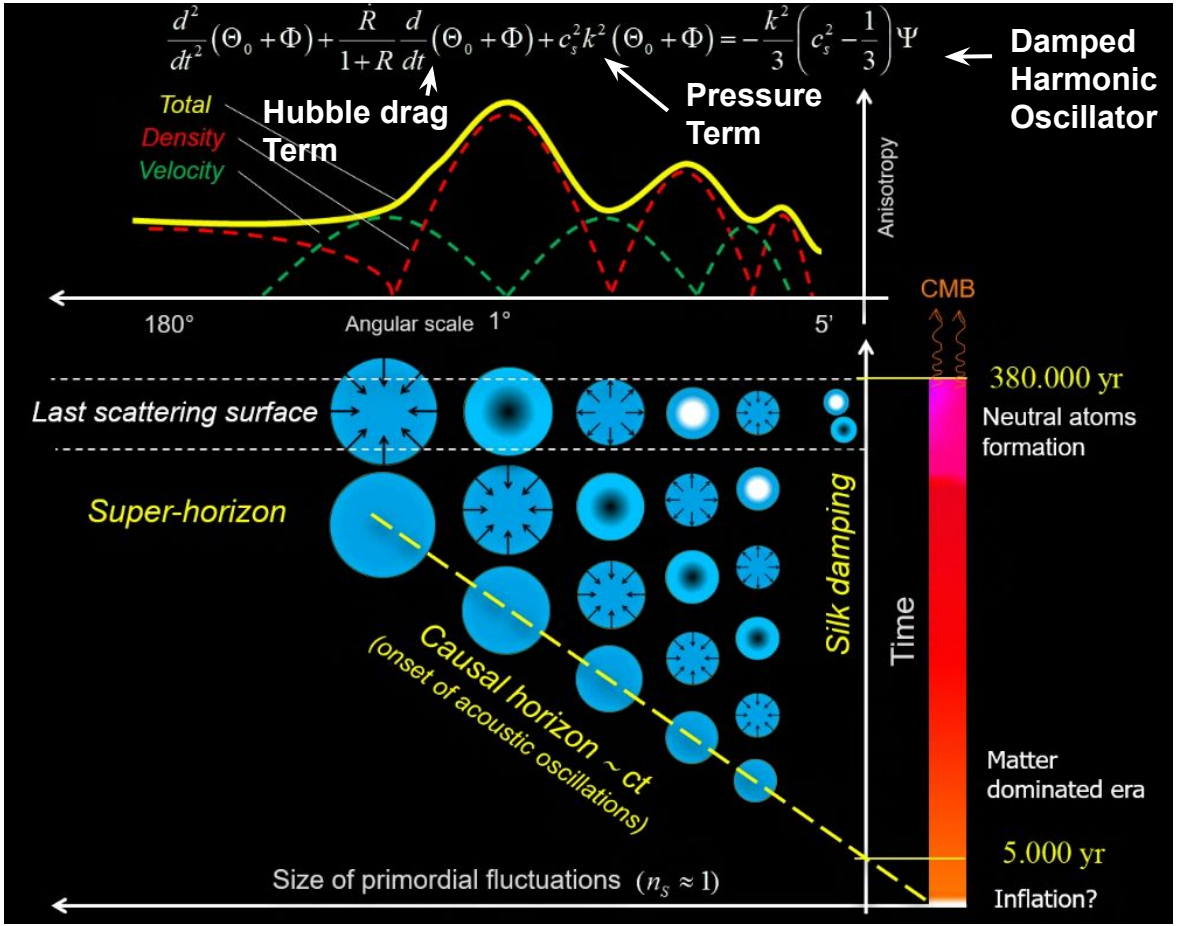

COSMIC MICROWAVE BACKGROUND RADIATION

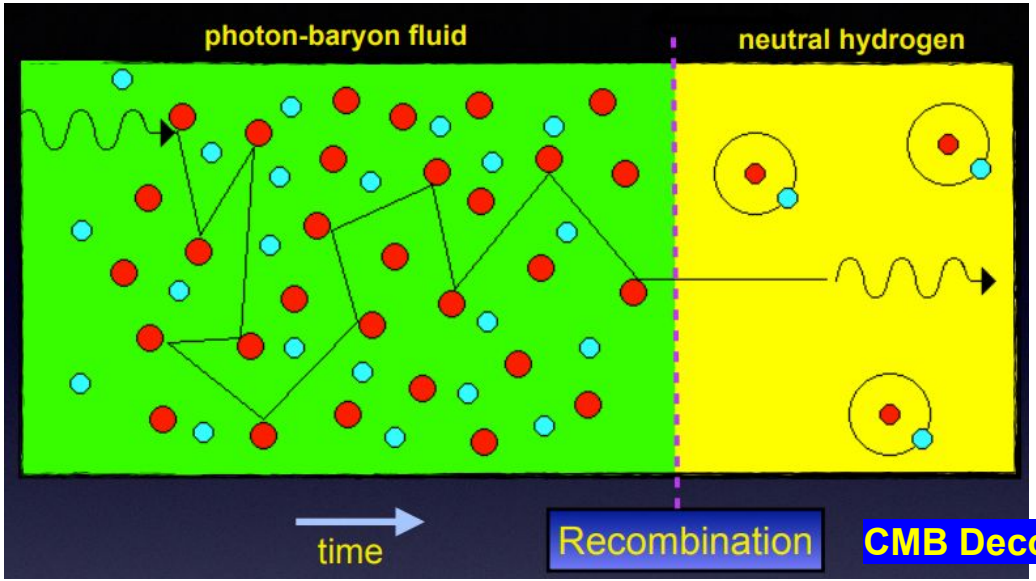

CMB radiation comes to us from last scattering surface (LSS). Since recombination is not instantaneous, in general $z_{LSS} \neq z_{rec} \simeq 1090$. Here, the redshift of recombination, is defined as the redshift at which the ionization fraction drops below some value (typically 0.1). Rather $z_{LSS} = z_{dec} \simeq 1080$, where the latter is the redshift of decoupling, defined as the epoch at which the Thomson scattering rate is equal to the Hubble expansion rate

COSMIC MICROWAVE BACKGROUND ANISOTROPIES

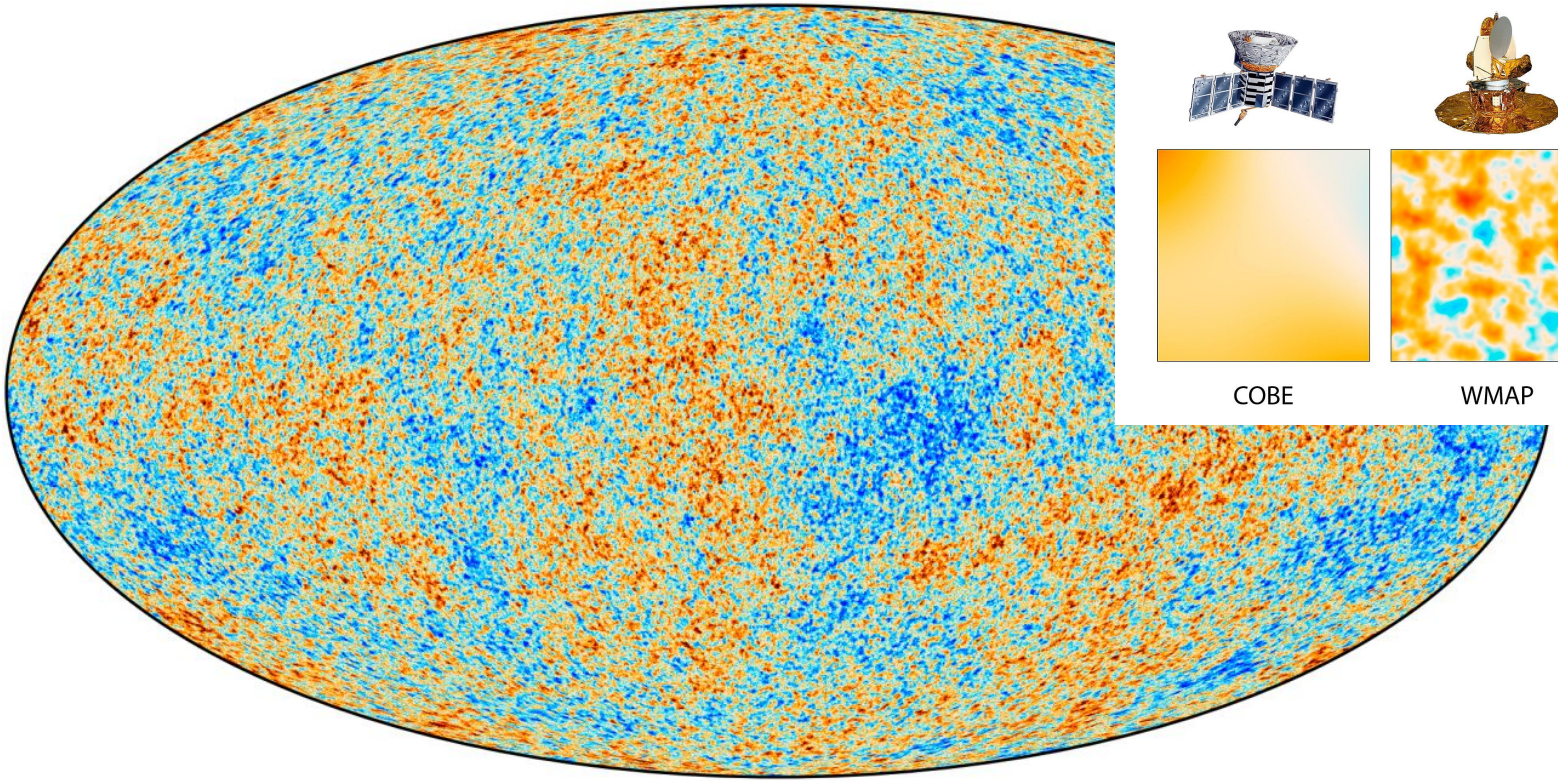

−300 μK 300

COSMIC MICROWAVE BACKGROUND ANISOTROPIES

Define the CMB anisotropy distribution

$$\Theta(\hat{n}) \equiv \frac{\Delta T}{T}(\hat{n}) = \frac{T(\hat{n}) - \bar{T}}{\bar{T}}$$

Here $\hat{n} = (\vartheta, \phi)$ is direction on the sky, and $\bar{T}$ is the average CMB temperature.

We expand this in Spherical Harmonics:

$$\Theta(\hat{n}) = \sum_{l,m} a_{lm}\, Y_{lm}(\vartheta, \phi)$$

and define the power spectrum as

$$\mathcal{C}_l = \langle |a_{lm}|^2 \rangle$$

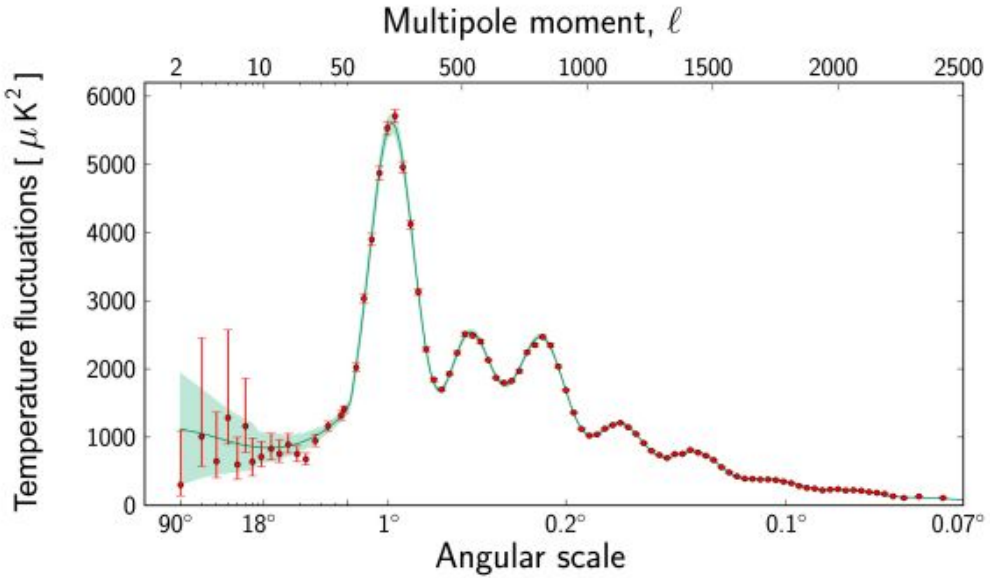

COSMIC MICROWAVE BACKGROUND ANISOTROPIES

An important angular scale is that corresponding to the comoving Hubble radius at decoupling, $r_H = c/H(z_{dec})$:

$$\theta_H = \frac{r_H}{d_A(z_{\rm dec})(1+z_{\rm dec})} \simeq 0.87^\circ$$

Which corresponds to $\ell \simeq 200$; CMB anisotropies with $\ell < 200$ correspond to super-horizon scale perturbations. On these super-horizon scales, only two effects can contribute to non-zero $\Delta T/T$ fluctuations:

i) fluctuations of the photon density at decoupling
ii) fluctuations in the gravitational potential (photons lose energy when climbing out of a potential well)

The combination of these two effects is known as the Sachs-Wolfe effect

The relation between ℓ and the associated angular scale ϑ is: $\theta \sim \frac{\pi}{\ell}\mathrm{rad} \sim \frac{180^\circ}{\ell}$

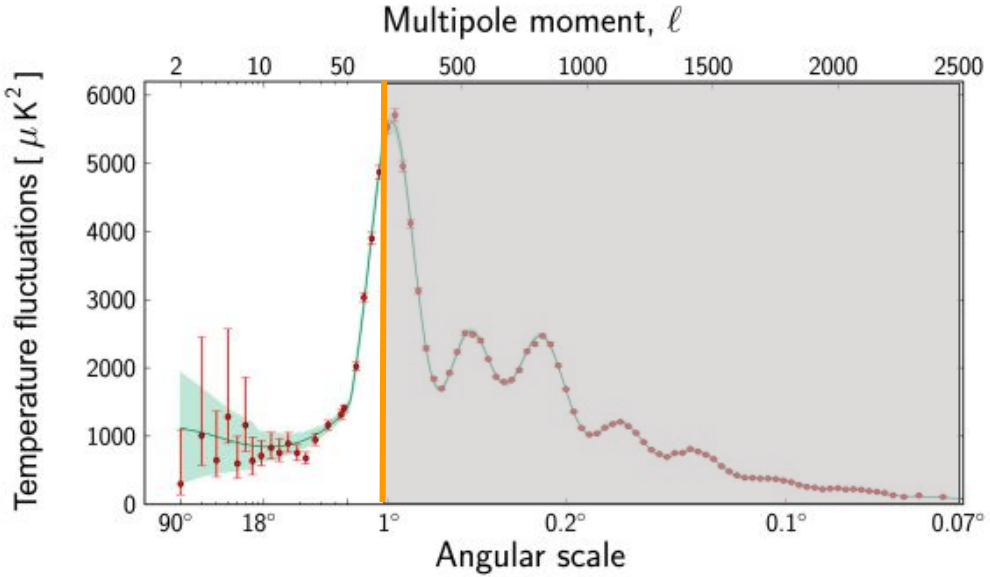

CMB ACOUSTIC PEAKS

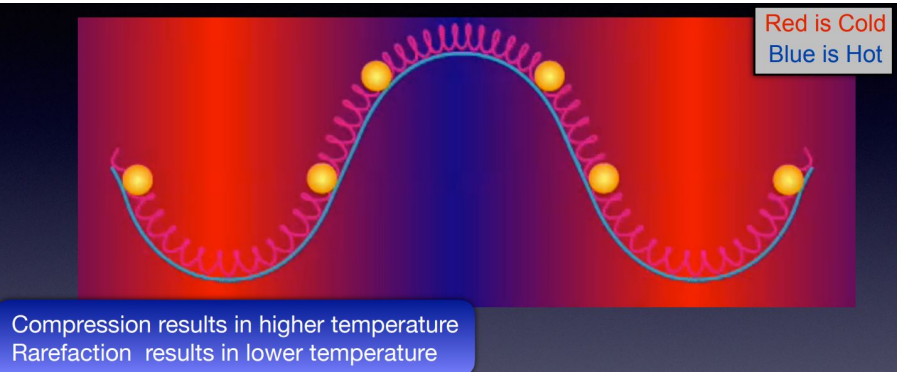

On sub-horizon scales the rich structure observed in the temperature anisotropy spectrum is mainly a consequence of the acoustic oscillations of the tightly-coupled baryon-photon fluid in the pre-recombination era. Perturbations in the gravitational potential, dominated by the CDM component, drive the oscillations in the plasma, with photon pressure, due to Thomson scattering of photons off free electrons, providing most of the restoring force.

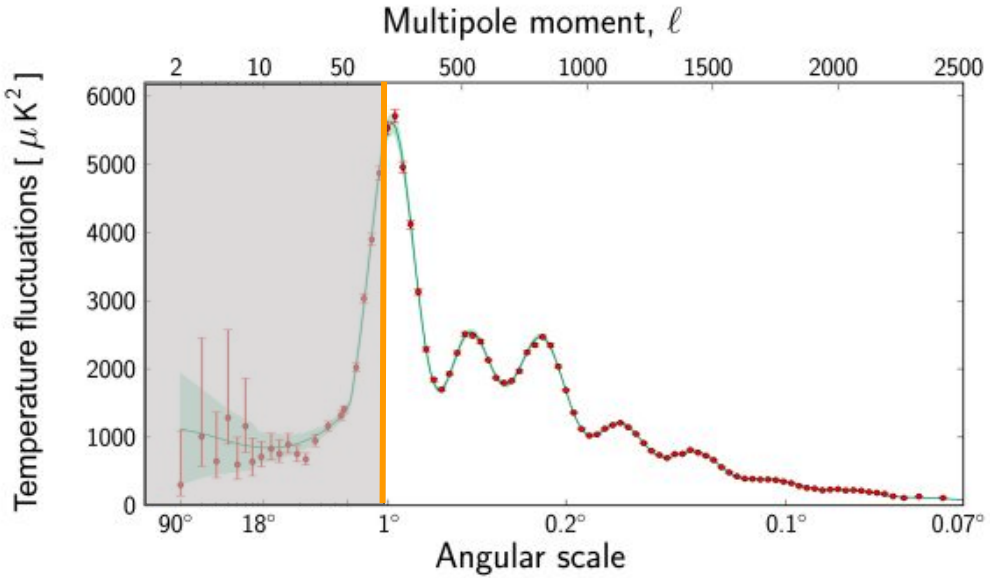

After recombination, photons can travel freely toward us, and the phases of the oscillations is imprinted in the CMB spectrum as a series of harmonic peaks. The last-scattering surface is a snapshot view of oscillation phases of all different modes.

CMB ACOUSTIC PEAKS

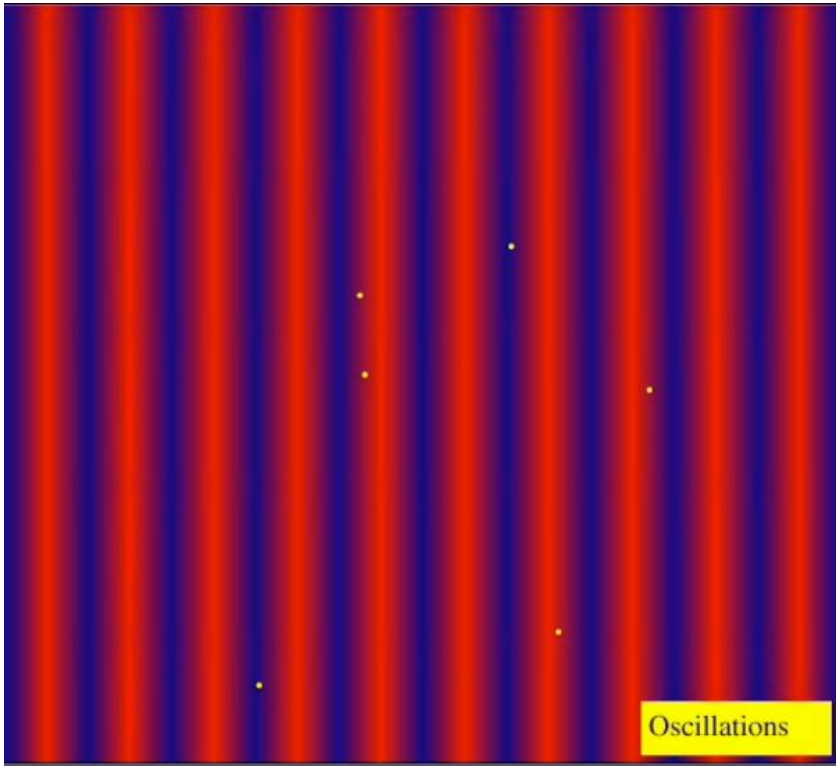

If we consider a single perturbation mode

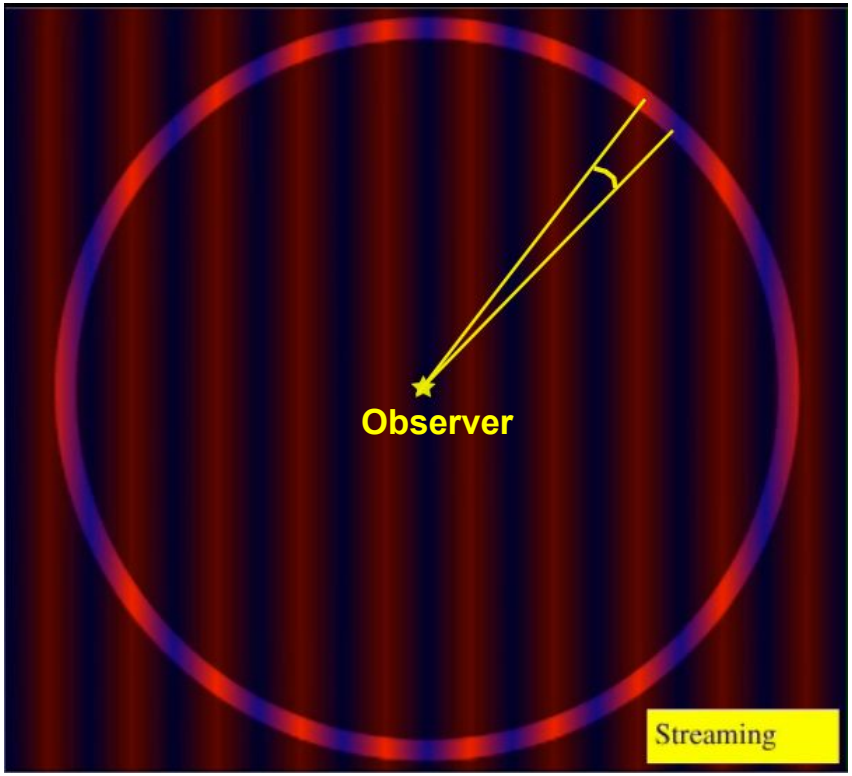

The observer sees this mode as angular temperature fluctuation on the sky, with a characteristic angular scale set by the wavelength of the mode

CMB ACOUSTIC PEAKS

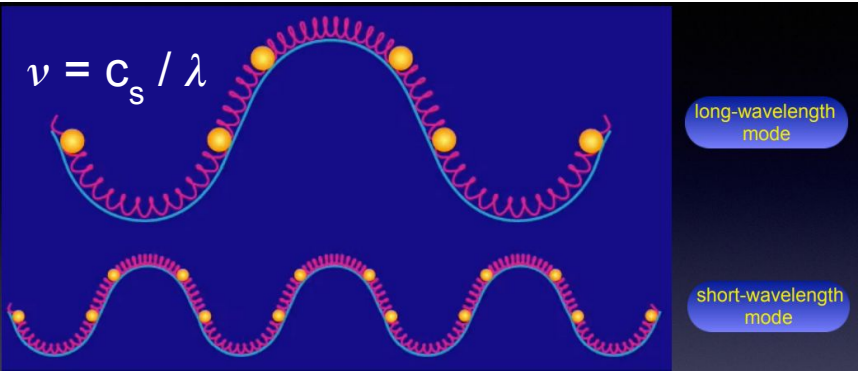

Since sound speed of photon-baryon fluid is the same for all modes, those with a smaller wavelengths oscillate faster.

The first peak corresponds to the mode that is caught in its first compression by recombination. The second peak corresponds to the mode that went through a full cycle of compression and rarefaction by recombination. The even peaks are generally of smaller amplitude because the rebound has to fight against baryon inertia.

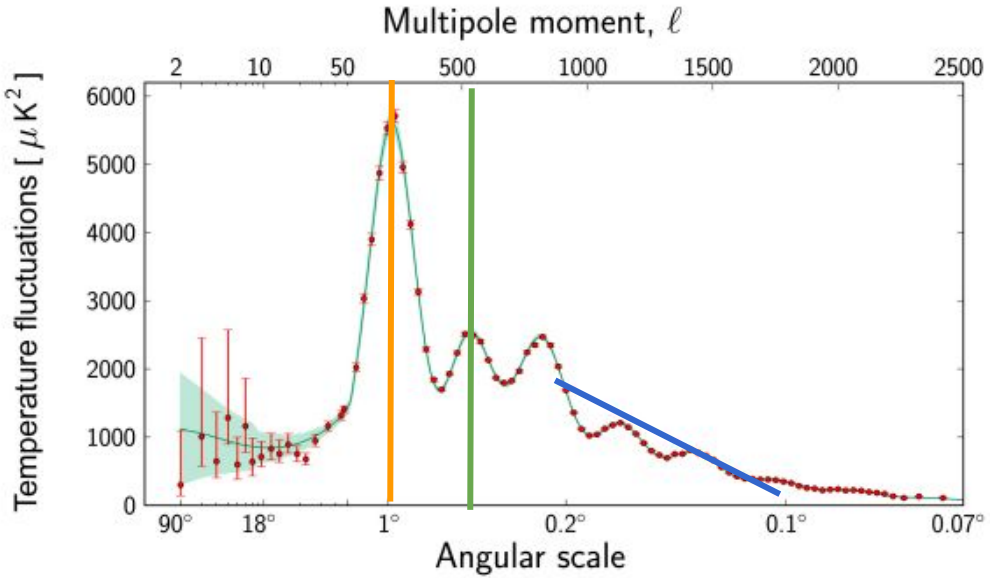

Damping tail: On small scales photon diffusion suppresses density fluctuations (Silk damping). Moreover, since the recombination process is not instantaneous, the last scattering surface has a finite thickness. This leads to a smearing of the anisotropies on scales smaller than the width ($\Delta z \approx 80$) of the recombination process, $\ell > 1000$.

CMB SECONDARY ANISOTROPIES

At angular scales smaller than few arc-minutes CMB temperature fluctuations are no longer dominated by primary effects at the surface of last scattering, but rather by the so-called secondary anisotropies which arise from the interaction of the CMB photons with the matter along the line of sight. The secondary anisotropies can be divided in two major families depending on the physical process which generate them. *The first family arises from the interaction of the photons with gravitational potential wells*, and it includes gravitational lensing and the late ISW effect. As for former, the gravitational deflection of CMB photons by intertwining non-linear structures causes a smoothing of the acoustic peaks up to 10% level at $\ell >$ 2000, and generate small-scale power that dominates the primary anisotropies for $\ell >$ 4000, where the diffusion damping is highly effective. Moreover, CMB lensing introduces non-Gaussianity in the four-point correlation function with a very specific and predictable shape, from which it is possible to reconstruct the power spectrum of the lensing potential (see later). *The second family incorporates the effects of scattering of CMB photons with free electrons,* such as reionization effects and the Sunyaev and Zeldovich effect (see previous slides).

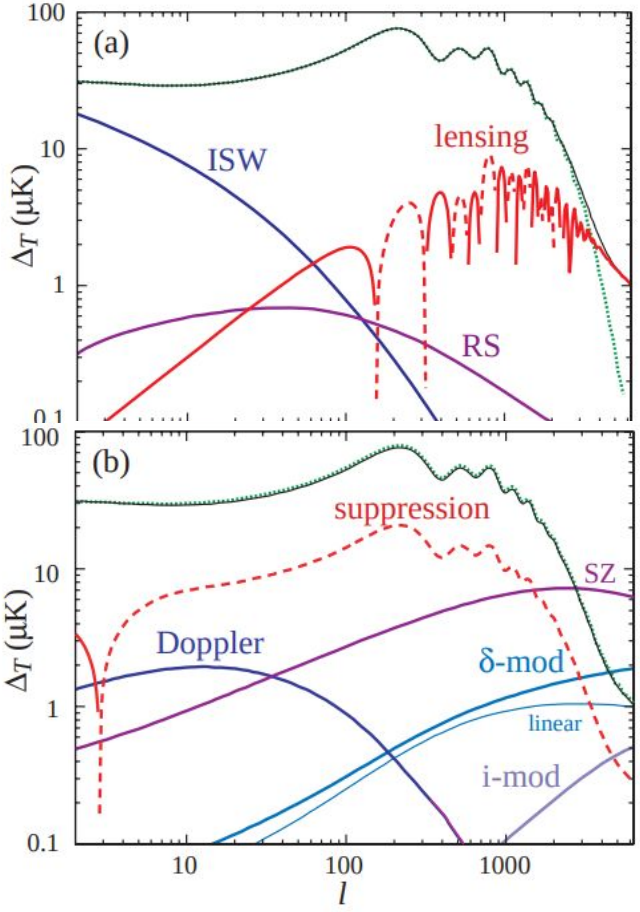

Credit: Hu & Dodelson 2002

CMB TEMPERATURE POWER SPECTRUM

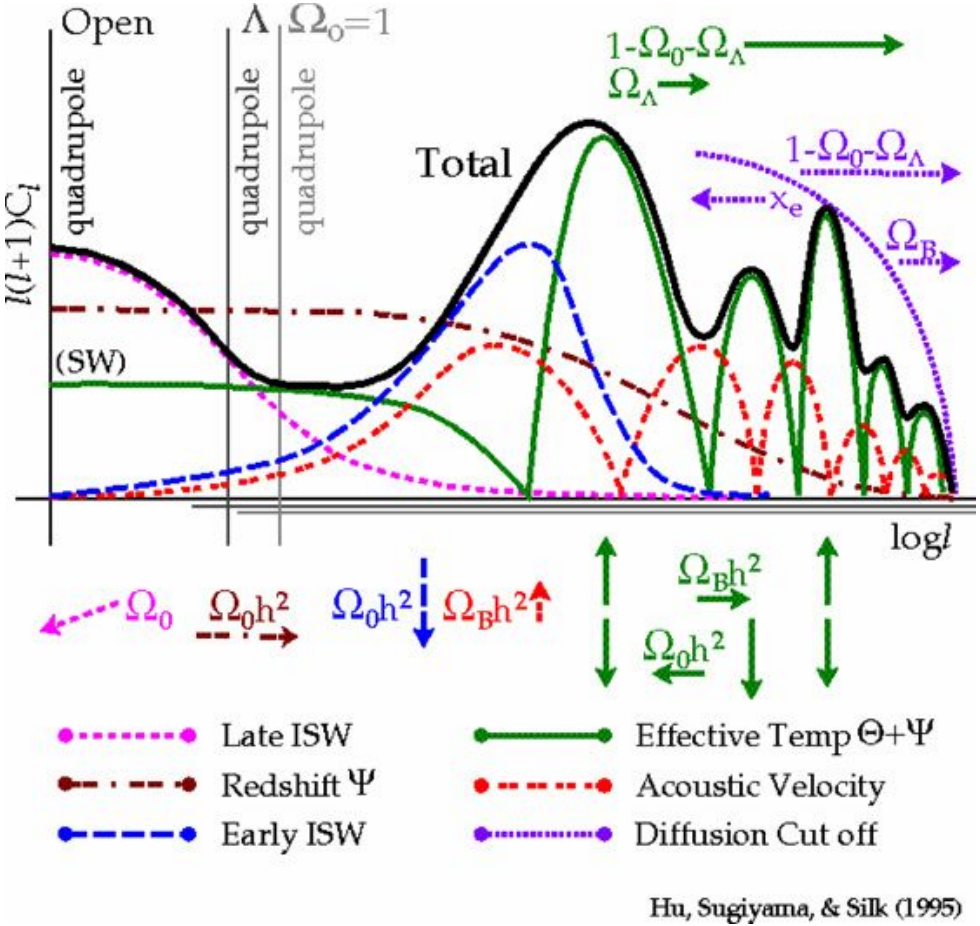

Contributions to the CMB temperature power spectrum of various physical processes and their dependence on Ω_m , Ω_b , Ω_Λ . Features in open models ($\Omega_k = 1 - \Omega_m - \Omega_\Lambda > 0$) are shifted to larger *l* compared to flat ΛCDM (Λ) or EdS ($\Omega_m = 1$) models, represented here as a shift of the origin of the x-axis (ℓ=2 quadrupole). Contributions from different physical processes are shown with different line styles (see legend). The arrows indicate the direction of change of the various contribution led by the increase of the model parameter written aside. For example, an increase of $\Omega_b h^2$ increases the heights of the first and third acoustic peaks, shifts the peaks to larger *l* and increases the overall contribution of the acoustic velocity peaks.

On line CMB spectrum: link

CMB TEMPERATURE POWER SPECTRUM

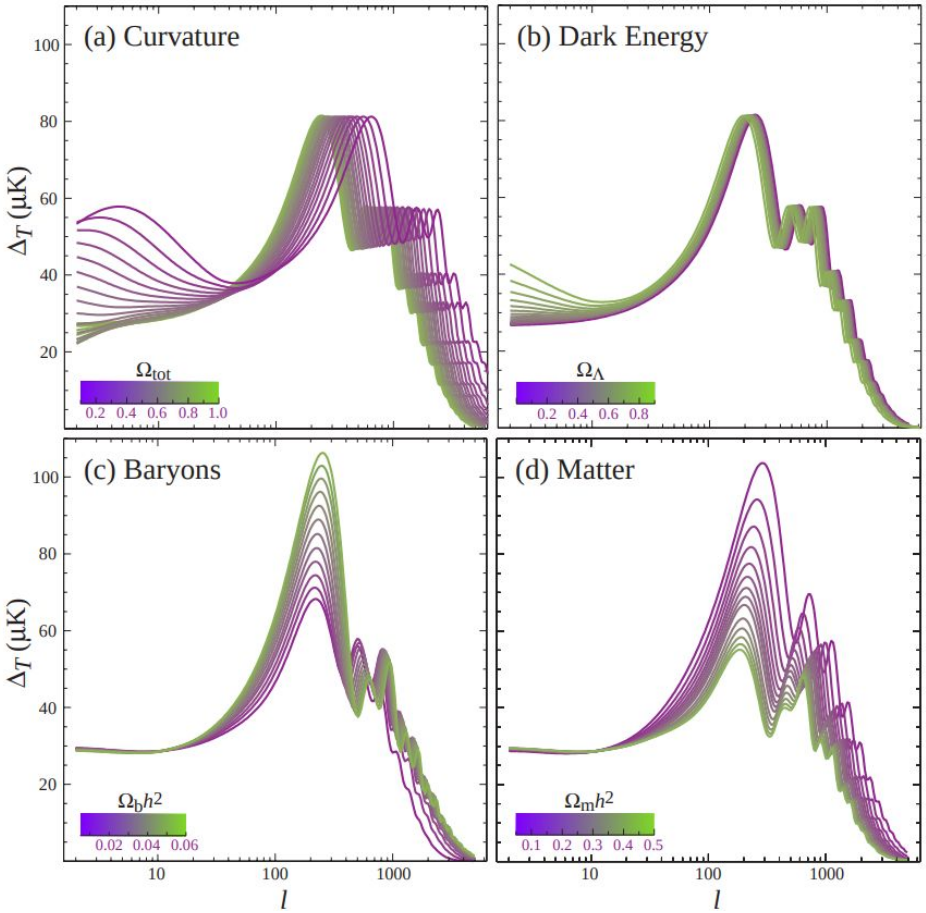

Credit: Hu & Dodelson 2002

The *position* of the acoustic peaks are determined by the physical size of the sound horizon at decoupling, and the angular diameter distance of the last scattering surface. Thus, the position of the peaks depends on the geometry of the space and on the value of Ω_b. Furthermore, the value of Ω_b controls also the relative amplitude between even and odd peaks and the depth of the valleys. In addition, the heights of the acoustic peaks can be affected by the strength of the initial perturbations (A_s and n_s) , and by Ω_m through the time evolution of the gravitational potential induced by the self-gravity of the acoustic perturbations.

CMB POLARIZATION POWER SPECTRUM

Thomson scattering of a radiation field with a quadrupole anisotropy produces linear polarization. The relevant epoch for the generation of polarization in the CMB is around recombination since at early times scattering is too efficient to allow a significant quadrupole to grow, while after recombination scatterings are very rare (until the universe reionizes).

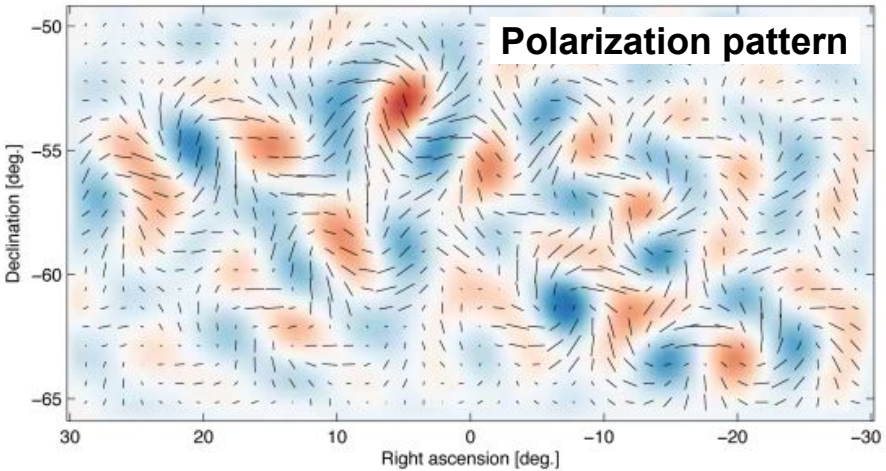

From acoustic density perturbations

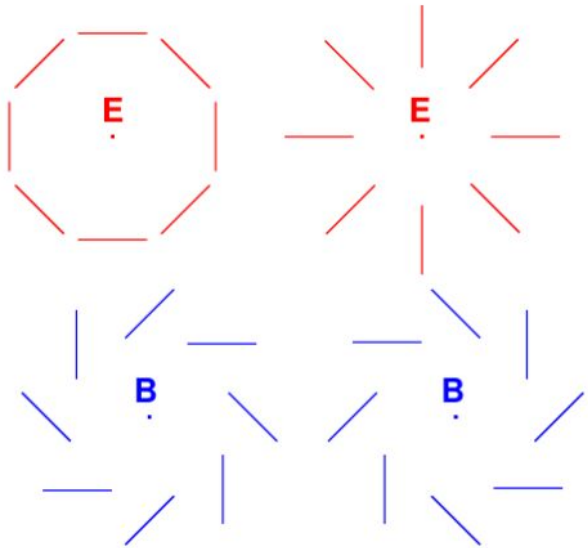

From primordial gravitational waves or lensing

For a review: https://arxiv.org/pdf/2412.04099

CMB POLARIZATION POWER SPECTRUM

The CMB polarization signal is expected to have a r.m.s. of ~ 5μK, peaking at multipoles l ≃ 1000 (*the angle subtended by the photon mean free path at last scattering*). The amplitude of the polarization signal is much smaller than the temperature power spectrum.

B-mode polarization can be induced by tensor perturbation, generated by the primordial gravitational waves predicted in the inflationary scenario, or by gravitational lensing due to the intertwining structures along the line of sight. A measurement of the gravitational waves power probes directly the energy scale of inflation.

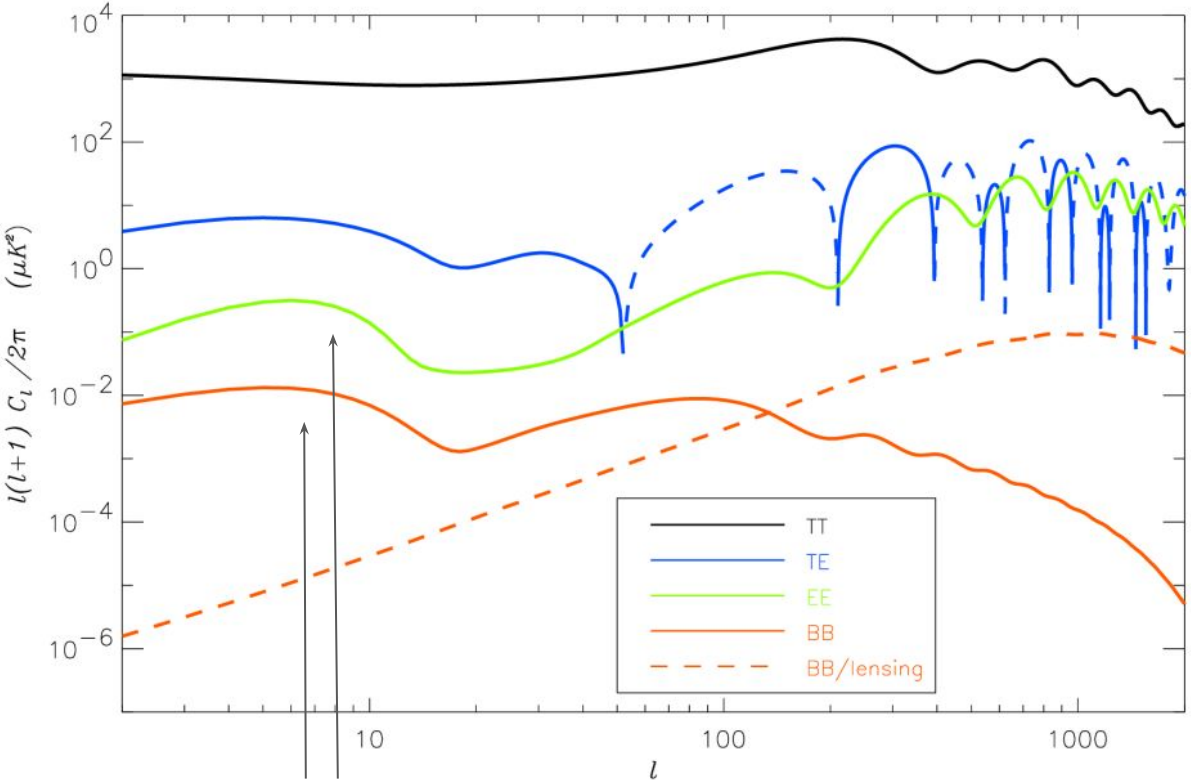

The "bump" at low multipoles (l< 20) in the polarization spectra is due to the re-scattering of CMB photons at reionization. The position of this peak is set by the size of the horizon at reionization, while its amplitude is determined by the duration of the ionization process.

CMB POLARIZATION

EE, TE Power Spectra:

- Polarization variations occur primarily on small scales. On scales larger than the **photon diffusion length** (the distance a photon travels between scatterings), photons from hot and cold regions haven't "mixed" enough to create the necessary quadrupole.
- EE peaks near the diffusion scale (l~1000, Recombination Peak) at a level that represents <10% polarization of the anisotropies and hence a several micro Kelvin signal.
- It has a second peak on large angular scales (Reionization bump) representing the same Thomson scattering process but arising after the epoch of reionization. This signature is on large angles since the photons diffuse across the whole visible Universe today. The signal is very faint (0.1 μK since the probability of a CMB photon scattering in recent times is a the percent level and below.

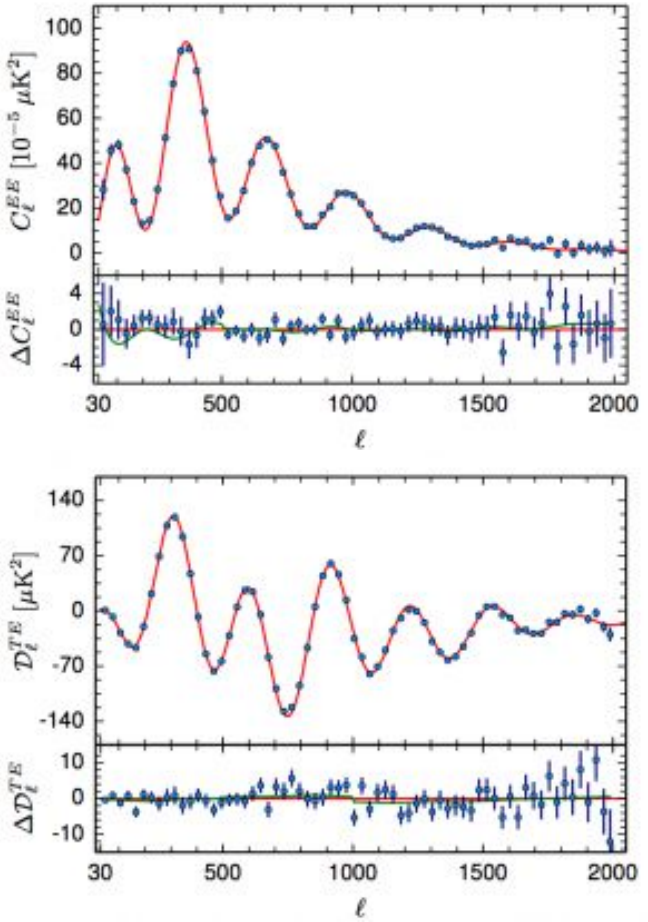

CMB POLARIZATION

EE, TE Power Spectra:

- EE Polarization power also exhibits acoustic oscillations since the quadrupole anisotropies that generate it are themselves formed from the acoustic motion of the fluid.
- Because polarization tracks the **velocity** of the plasma (rather than just the density/pressure), the peaks in the EE and TE spectra are **out of phase** with the Temperature (TT) peaks. When the plasma density is at a maximum or minimum (TT peak), the velocity is zero (EE trough)

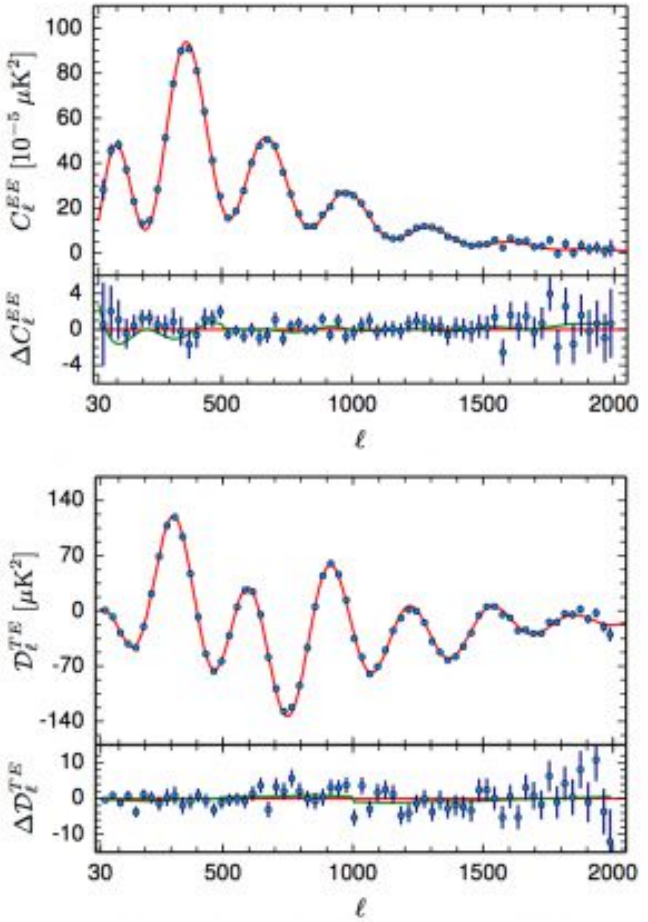

CONSTRAINTS FROM CMB DATA

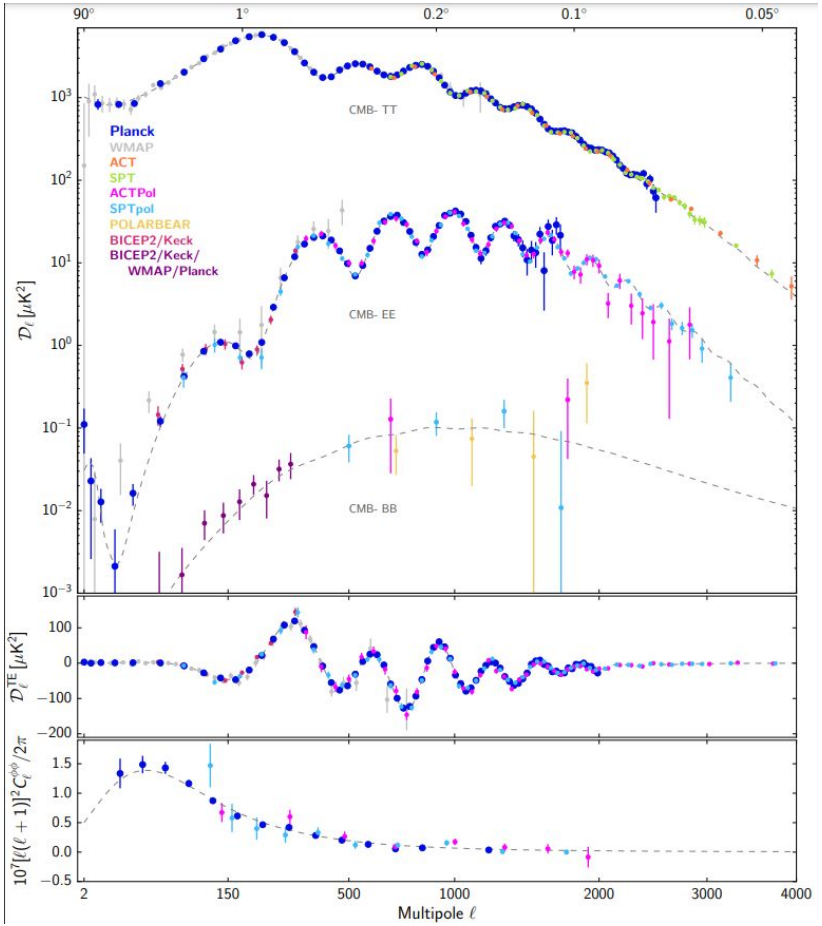

Nowadays CMB data (temperature and polarization) provides the single-probe tighter constraints on the ΛCDM model parameters.

All sky surveys, like Planck, are cosmic variance limited (especially at the largest scale, low ℓ). Combining CMB experiments with different angular resolution and sky coverage allow to improve the constraining power by increasing the multipole range that can be probed (e.g. Planck and SPT)

	SPT-3G 2018	SPT-3G 2018 + *Planck*
$\Omega_b h^2$	0.02224 ± 0.00032	0.02233 ± 0.00013
$\Omega_c h^2$	0.1166 ± 0.0038	0.1201 ± 0.0012
$100\theta_{MC}$	1.04025 ± 0.00074	1.04075 ± 0.00028
$10^9 A_s e^{-2\tau}$	1.871 ± 0.030	1.884 ± 0.010
n_s	0.970 ± 0.016	0.9649 ± 0.0041
$H_0\ [\mathrm{km\,s^{-1}\,Mpc^{-1}}]$	68.3 ± 1.5	67.24 ± 0.54
σ_8	0.797 ± 0.015	0.8099 ± 0.0067
$S_8 \equiv \sigma_8 \sqrt{\Omega_m/0.3}$	0.797 ± 0.042	0.832 ± 0.014
Ω_Λ	0.700 ± 0.021	0.6835 ± 0.0075
Age/Gyr	13.815 ± 0.047	13.807 ± 0.021

CONSTRAINTS FROM CMB DATA

https://arxiv.org/pdf/2212.05642.pdf

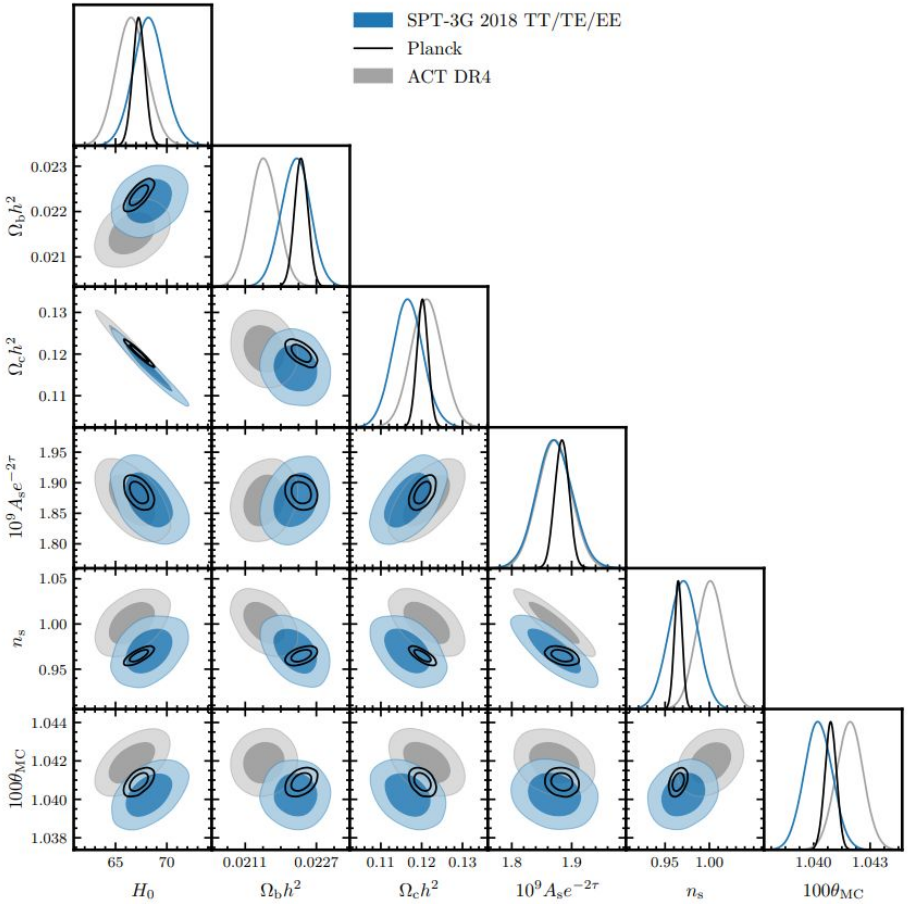

Nowadays CMB data (temperature and polarization) provides the single-probe tighter constraints on the ΛCDM model parameters.
All sky surveys, like Planck, are cosmic variance limited (especially at the largest scale, low ℓ).
Combining CMB experiments with different angular resolution and sky coverage allow to improve the constraining power by increasing the multipole range that can be probed (e.g. Planck and SPT)

	SPT-3G 2018	SPT-3G 2018 + *Planck*
$\Omega_b h^2$	0.02224 ± 0.00032	0.02233 ± 0.00013
$\Omega_c h^2$	0.1166 ± 0.0038	0.1201 ± 0.0012
$100\theta_{MC}$	1.04025 ± 0.00074	1.04075 ± 0.00028
$10^9 A_s e^{-2\tau}$	1.871 ± 0.030	1.884 ± 0.010
n_s	0.970 ± 0.016	0.9649 ± 0.0041
H_0 [km s^{-1} Mpc^{-1}]	68.3 ± 1.5	67.24 ± 0.54
σ_8	0.797 ± 0.015	0.8099 ± 0.0067
$S_8 \equiv \sigma_8 \sqrt{\Omega_m/0.3}$	0.797 ± 0.042	0.832 ± 0.014
Ω_Λ	0.700 ± 0.021	0.6835 ± 0.0075
Age/Gyr	13.815 ± 0.047	13.807 ± 0.021

tSZ POWER SPECTRUM

Dependence on cosmological parameters:

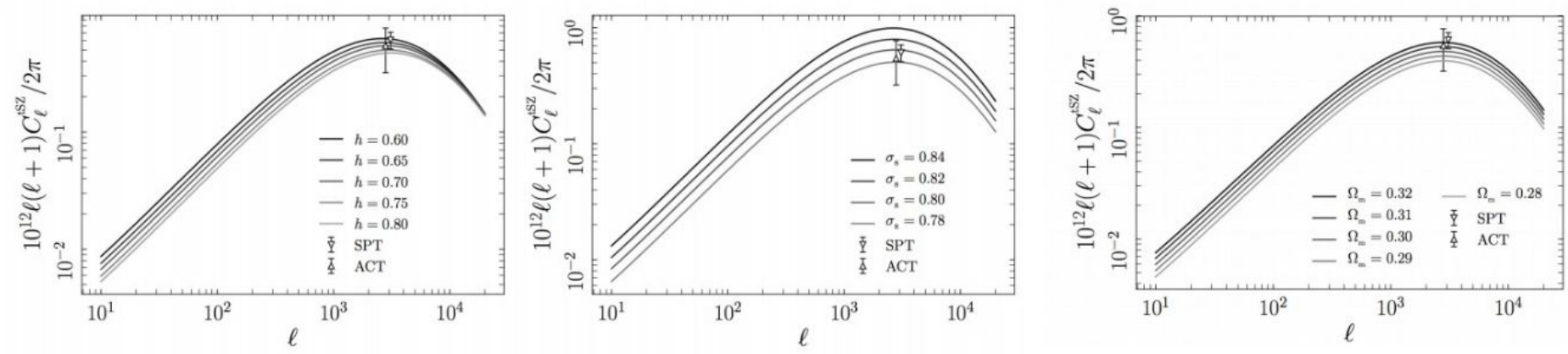

- **On large scale the amplitude scale as:**

$$C_\ell^{\rm tSZ} \propto \sigma_8^{8.1}\Omega_{\rm m}^{3.2}B^{-3.2}h^{-1.7}$$

B = hydrostatic mass bias

- **Due to large degeneracies we can actually constrain the parameter combination:**

$$F \equiv \sigma_8(\Omega_{\rm m}/B)^{0.40}h^{-0.21}$$

tSZ POWER SPECTRUM

Dependence on cosmological parameters:

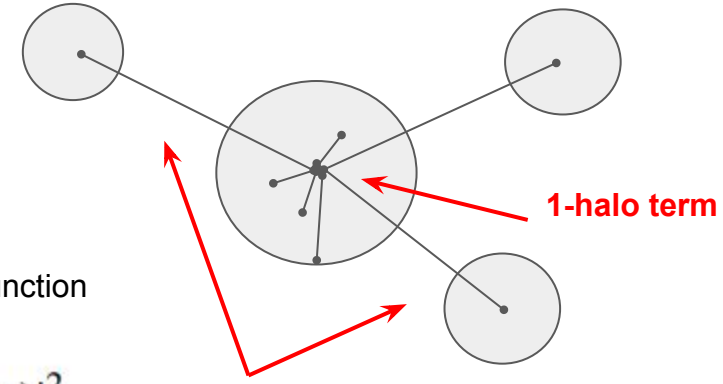

$$C_\ell^{SZ} = C_\ell^{1halo} + C_\ell^{2halos}$$

$$C_\ell^{1halo} = \int_0^{z_{max}} dz \frac{dV_c}{dz d\Omega} \int_{M_{min}}^{M_{max}} dM \frac{dn(M,z)}{dM} |\tilde{y}_\ell(M,z)|^2$$

Halo mass function

FT of radial compton-y profile of individual clusters

$$C_\ell^{2halos} = \int_0^{z_{max}} dz \frac{dV_c}{dz d\Omega} \times \left[\int_{M_{min}}^{M_{max}} dM \frac{dn(M,z)}{dM} |\tilde{y}_\ell(M,z)| \; B(M,z) \right]^2 P(k,z)$$

Halo bias

Matter power spectrum

tSZ POWER SPECTRUM

Dependence on cosmological parameters: impact of hydrostatic mass bias

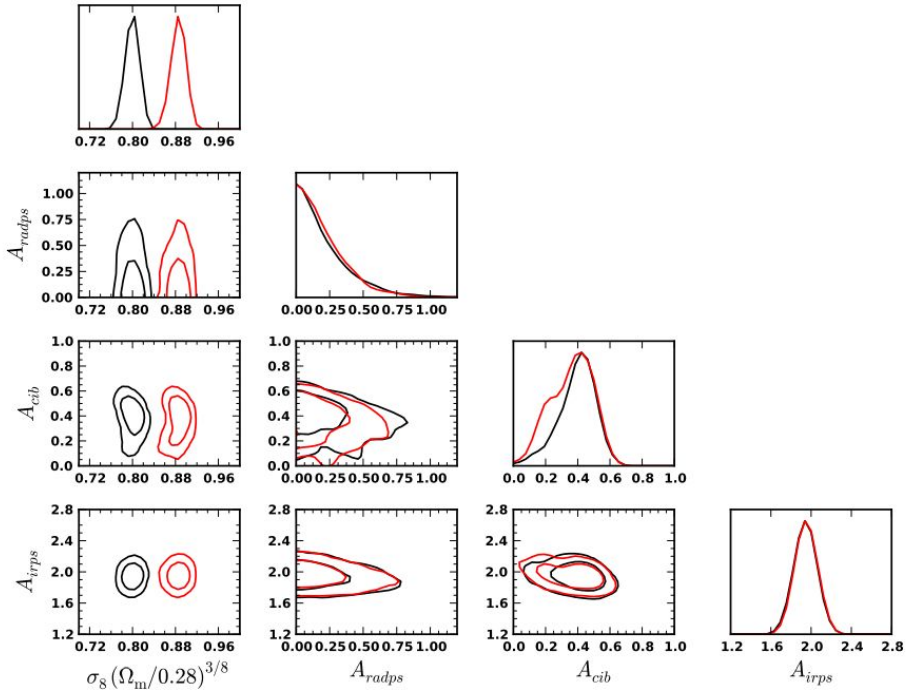

Planck 2015 results

Fig. 16: 2D and 1D likelihood distributions for the combination of cosmological parameters $\sigma_8(\Omega_{\rm m}/0.28)^{3/8}$, and for the foreground parameters $A_{\rm Rad.PS}$, $A_{\rm CIB}$ and $A_{\rm IR.PS}$. We show the 68.3% and 95.4% C.L. contours. The red and black contours correspond to a fixed mass bias of 0.2 and 0.4 respectively.

STATISTICAL PROPERTIES OF THE LARGE SCALE STRUCTURES:

COSMIC SHEAR

For a review: https://arxiv.org/pdf/1201.2434.pdf **(Sec 5)**
https://arxiv.org/pdf/1612.06535.pdf
https://arxiv.org/pdf/0805.0139.pdf
https://arxiv.org/pdf/astro-ph/9912508.pdf

GRAVITATIONAL LENSING

Gravitational lensing: Light's path is deflected by the gravitational potential wells of cosmic structures crossed along its journey toward us.

This leads to:

- **Change of the apparent positions of the sources**
- **Distorsion (shear) of source images**
- **Magnification of the source images**

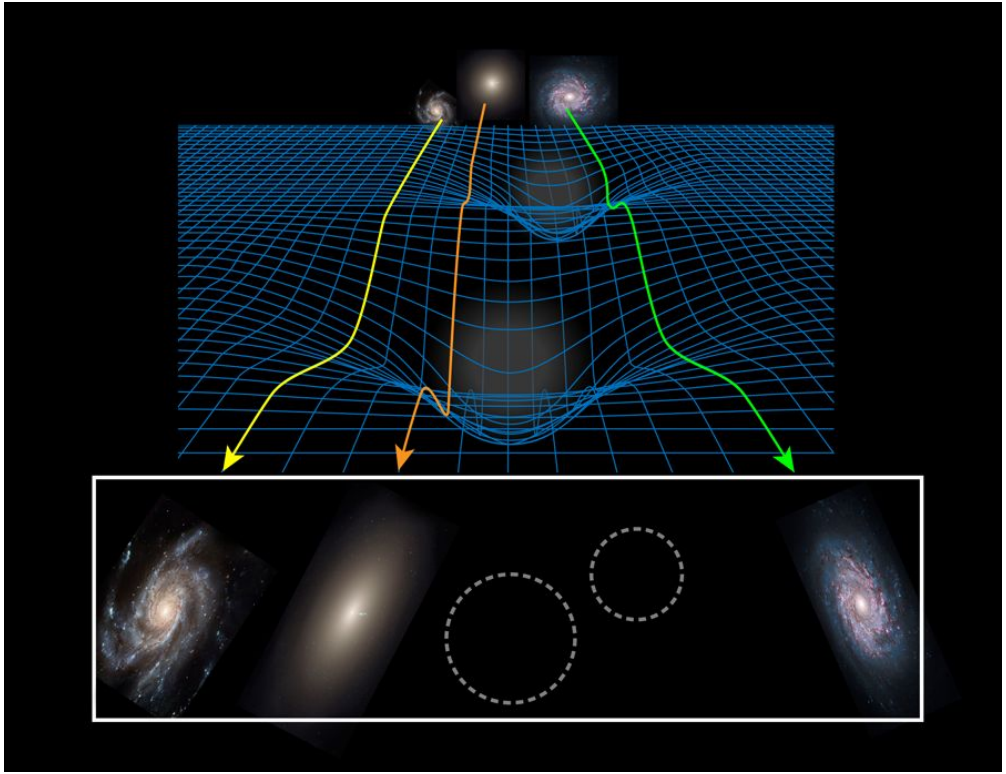

STRONG AND WEAK GRAVITATIONAL LENSING

Strong lensing:

- **Multiple images of the same source**
- **Strong distortions and magnification**

Weak lensing:

- **Shape distorted, stretched or magnified**
- **Detectable only statistically**

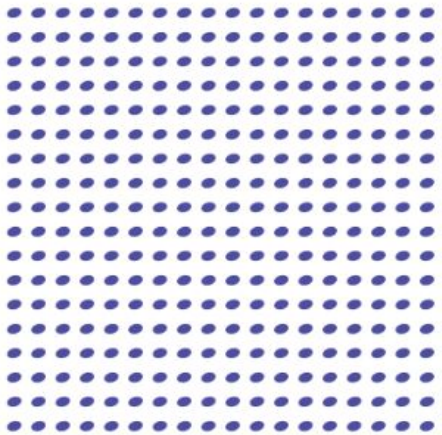

Unlensed sources

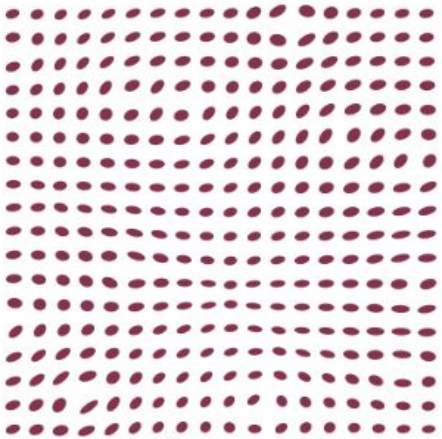

Weak lensing

GRAVITATIONAL LENSING: LENS EQUATION

- **Deflection of light ray by a gravitational potential fluctuation Φ:**

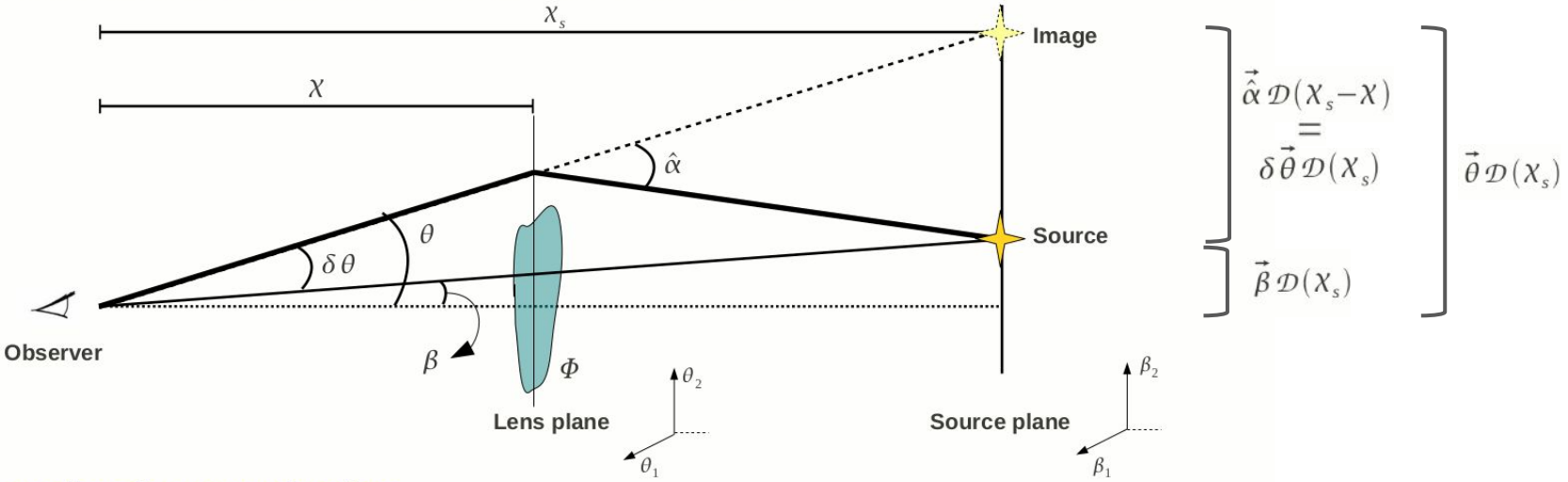

- **Using small angles approximation:**

$$\vec{\beta}\,\mathcal{D}(\chi_s)=\vec{\theta}\,\mathcal{D}(\chi_s)-\vec{\hat{\alpha}}\,\mathcal{D}(\chi_s-\chi)$$

- **Lens equation:**

$$\vec{\beta}=\vec{\theta}-\delta\vec{\theta} \qquad \text{with:} \quad \delta\vec{\theta}=\frac{\mathcal{D}(\chi_s-\chi)}{\mathcal{D}(\chi_s)}\vec{\hat{\alpha}} \qquad \textbf{(Scaled deflection angle)}$$

GRAVITATIONAL LENSING: LENS EQUATION

- **Perturbed metric:**

$$ds^2=\left(1+\frac{2\Phi}{c^2}\right)c^2dt^2-a^2(t)\left[\left(1-\frac{2\Phi}{c^2}\right)(d\chi^2+\mathcal{D}^2(\chi)d\Omega^2)\right]$$

n refractive index

Weak field approximation

- **Deflection angle:**

$$\vec{\hat{\alpha}}=\frac{2}{c^2}\int\nabla_\perp\Phi(\chi)d\chi$$

Thin lens approximation

Born approximation

- **Deflection angle of light ray arising from all the potential gradients between obs and source:**

$$\delta\vec{\theta}=\vec{\theta}-\vec{\beta}=\frac{2}{c^2}\int_0^{\chi_s}d\chi\frac{\mathcal{D}(\chi_s-\chi)}{\mathcal{D}(\chi_s)}\nabla_\perp\Phi(\chi)$$

- **Deflection potential:**

$$\psi(\vec{\theta},\chi_s)=\frac{2}{c^2}\int_0^{\chi_s}d\chi'\frac{\mathcal{D}(\chi_s-\chi)}{\mathcal{D}(\chi_s)\mathcal{D}(\chi)}\Phi(\mathcal{D}(\chi)\vec{\theta},\chi)$$

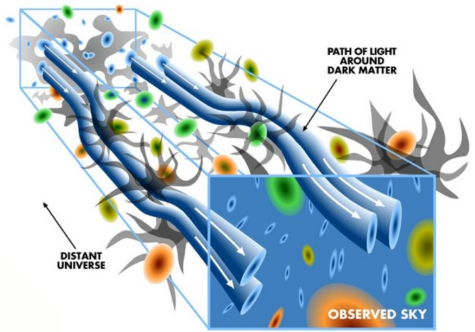

GRAVITATIONAL LENSING: κ and γ

- **Mapping of source image:**

Conservation of surface brightness

$$I(\vec{\theta}) = I^s(\vec{\beta}(\vec{\theta})) = I^s\left[\vec{\beta}(\vec{\theta}_0) + \mathcal{A}(\vec{\theta}_0)\cdot(\vec{\theta}-\vec{\theta}_0)\right]$$

Linearized lens mapping (Jacobi matrix):

$$\mathcal{A}(\vec{\theta}) = \frac{\partial\vec{\beta}}{\partial\vec{\theta}} = \left(\delta_{i,j} - \frac{\partial^2\psi(\vec{\theta})}{\partial\theta_i\partial\theta_j}\right) = \begin{pmatrix} 1-\kappa-\gamma_1 & -\gamma_2 \\ -\gamma_2 & 1-\kappa+\gamma_1 \end{pmatrix} =$$

$$= (1-\kappa)\begin{pmatrix} 1-g_1 & -g_2 \\ -g_2 & 1+g_1 \end{pmatrix} \qquad \text{with} \quad g(\boldsymbol{\theta}) = \frac{\gamma(\boldsymbol{\theta})}{[1-\kappa(\boldsymbol{\theta})]}$$

Convergence

$$\kappa = \frac{\psi_{,11}+\psi_{,22}}{2} = \frac{\nabla^2\psi}{2}$$

Shear

$$\gamma = \gamma_1 + \mathrm{i}\,\gamma_2 = |\gamma|\,\mathrm{e}^{2\mathrm{i}\varphi}$$

$$\gamma_1 = \frac{\psi_{,11}-\psi_{,22}}{2} \;;\; \gamma_2 = \psi_{,12}$$

- **Distortion of a circular image:**

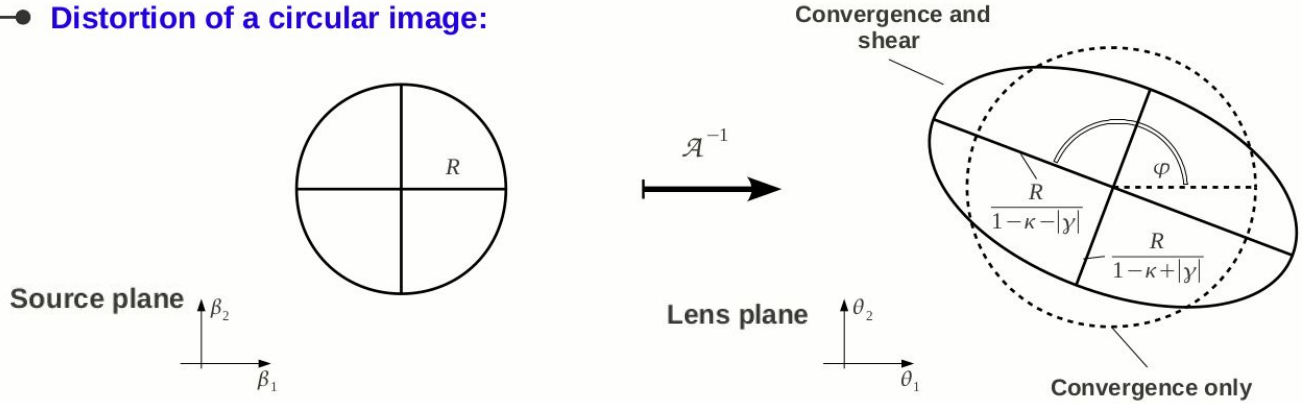

COSMIC SHEAR

Cosmic shear denotes tiny shape distortions (weak lensing) of distant galaxy images that arise from gravitational lensing of light by the LSS of the Universe.

The coherent distortion of background images (shear) can be related to the underlying matter density distribution:

$$\kappa(\vec{\vartheta}) = \int_0^{\chi_{\max}} \mathrm{d}\chi W(\chi)\delta(D_A(\chi)\vec{\vartheta},\chi)$$

Integral along the LOS

Angular convergence (or shear) power spectrum

$$C_{ij}(\ell) = \frac{\langle\hat{\kappa}(\boldsymbol{\ell})\hat{\kappa}^*(\boldsymbol{\ell}')\rangle}{(2\pi)^2\delta^D(\boldsymbol{\ell}-\boldsymbol{\ell}')} = \frac{\langle\hat{\gamma}(\boldsymbol{\ell})\hat{\gamma}^*(\boldsymbol{\ell})\rangle}{(2\pi)^2\delta^D(\boldsymbol{\ell}-\boldsymbol{\ell}')} = \int_0^{\chi_{\max}} \mathrm{d}\chi \frac{W_i(\chi)W_j(\chi)}{D_A(\chi)^2} P_\delta\left(\frac{\ell}{D_A(\chi)},\chi\right)$$

Lens efficiency, which depends on the geometry system

Matter power spectrum

From Hoekstra & Jain 2008

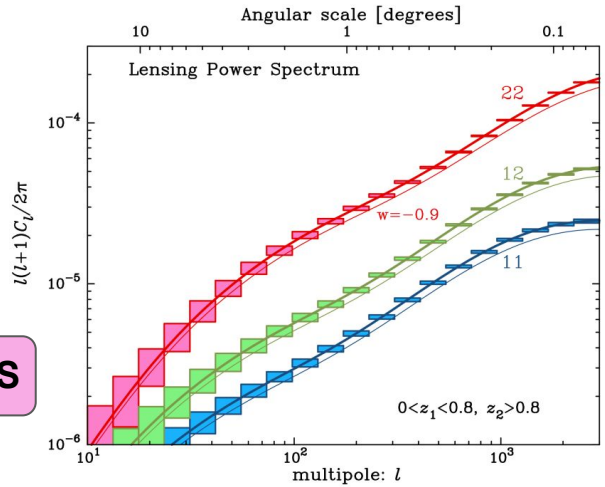

COSMIC SHEAR MEASUREMENT

The cosmic shear signal can be measured only statistically correlating the ellipticities of a large number of galaxies.

Second order cosmic shear measures:

Defining tangential and cross shear:

$$\gamma_t = -\Re[\gamma e^{-i2\phi}], \quad \gamma_\times = -\Im[\gamma e^{-i2\phi}]$$

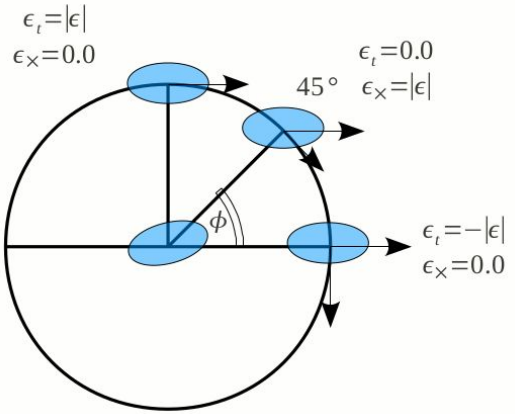

Rotationally invariant shear correlation function:

$$\xi_\pm(\theta) = \langle \gamma_t \gamma_t \rangle(\theta) \pm \langle \gamma_\times \gamma_\times \rangle, \quad \xi_\times(\theta) = \langle \gamma_t \gamma_\times \rangle(\theta)$$

Due to parity symmetry: $\xi_\times(\theta) = 0$

Relation with the power spectrum P_k:

$$\xi_\pm(\theta) = \int_0^\infty \frac{d\ell\,\ell}{2\pi} J_{0,4}(\ell\theta) P_\kappa(\ell)$$

$$P_\kappa(\ell) = 2\pi \int_0^\infty d\theta\,\theta\,\xi_\pm J_{0,4}(\ell\theta)$$

COSMIC SHEAR MEASUREMENT

The observed ellipticity of a galaxy, ϵ , is the result of the sum of its intrinsic ellipticity, ϵ^s , and the shear distortion, γ:

$$\xi_{\pm} = \langle \epsilon_i \epsilon_j^* \rangle = \xi_{\pm}^{lens} + \langle \epsilon_i^{(s)} \epsilon_j^{(s)*} \rangle + \langle \gamma_i \epsilon_j^{(s)*} \rangle + \langle \epsilon_i^{(s)} \gamma_j^* \rangle, \quad \text{with } z_i < z_j$$

Cosmic shear signal | Intrinsic alignment | ≡0 | Shape-shear correlation

- **Intrinsic alignments : Close pair of galaxies could be aligned by tidal forces of the DM structure surrounding them.**
- **Shape-shear correlation (Hirata & Seljak 2004): DM structure (gray) causes the alignment of nearby galaxy (blue) and contributes to the lensing signal of a background galaxy (red).**

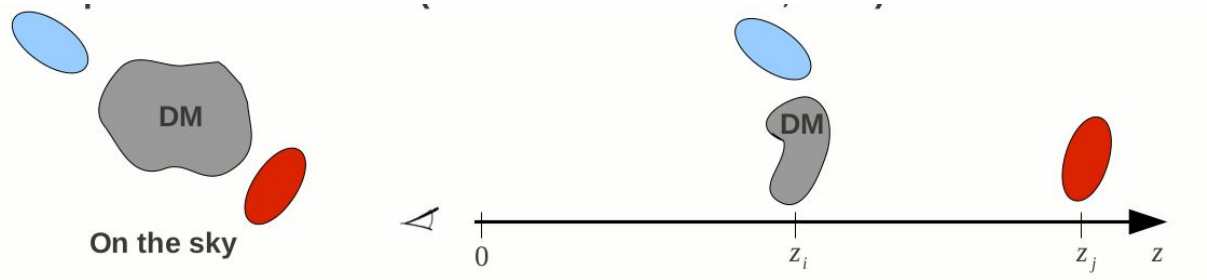

COSMIC SHEAR MEASUREMENT

The "forward" process of the source image:

Galaxies: Intrinsic galaxy shapes to measured image:

Intrinsic galaxy (shape unknown)

Gravitaional lensing causes a ***shear (g)***

In real data $g_i \sim 0.03$

Atmosphere and telescope cause a convolution

In real data Kernel size ~ galaxy size

Detectors measure a pixelated image

In real data Pixel size ~ (Kernel size) / 2

Image also contains noise

Mostly Poissonian.

Stars: Point sources to star images:

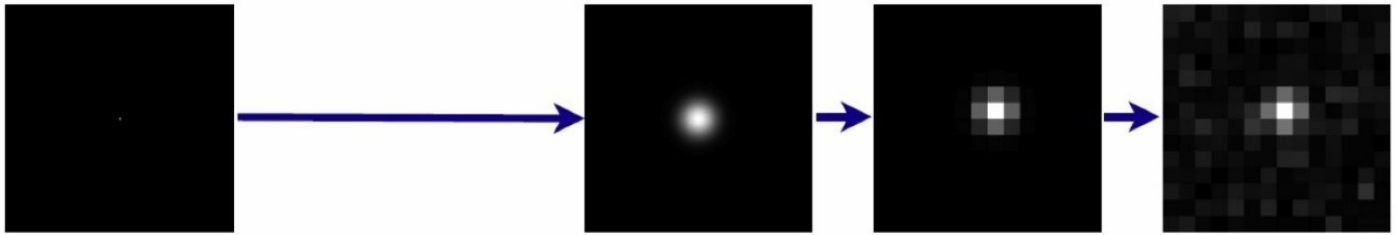

Intrinsic star (point source)

Atmosphere and telescope cause a convolution

Detectors measure a pixelated image

Image also contains noise

COSMIC SHEAR MEASUREMENT

The "forward" process of the source image:

Galaxies: Intrinsic galaxy shapes to measured image:

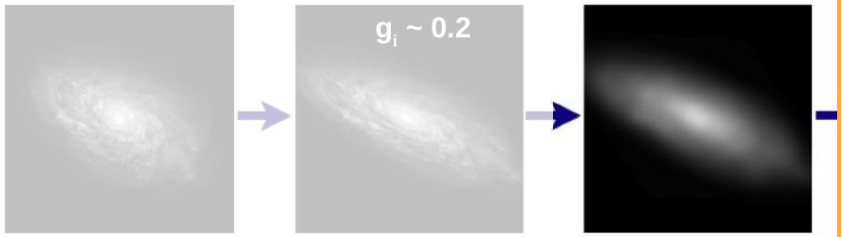

Intrinsic galaxy (shape unknown)

Gravitaional lensing causes a ***shear (g)***

In real data $g_i \sim 0.0$

Atmosphere and telescope cause a convolution

a pixelated image

contains noise

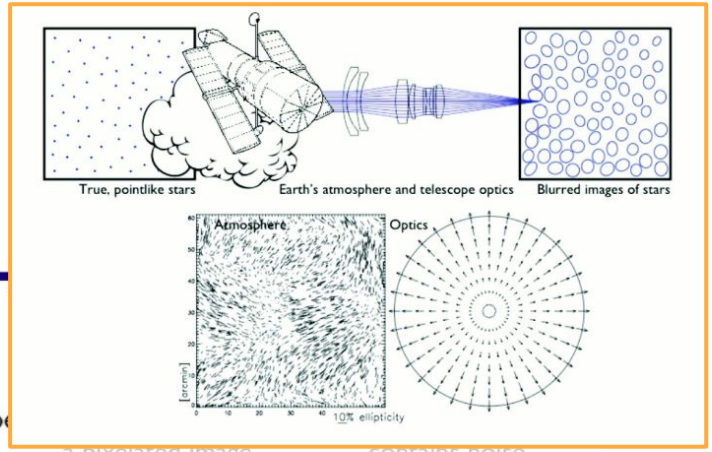

Stars: Point sources to star imag

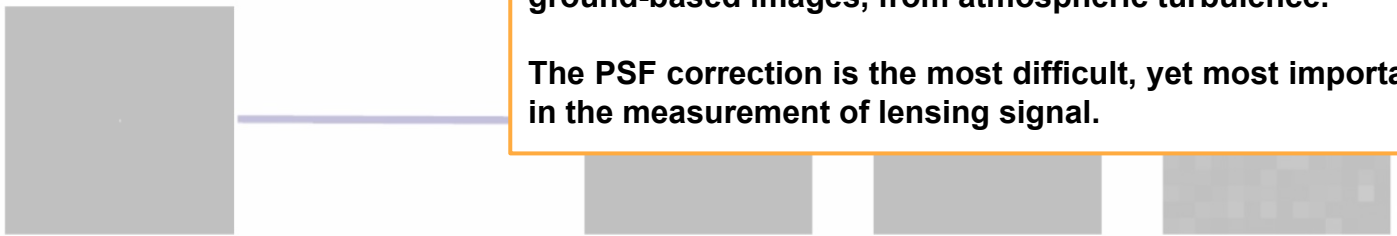

Intrinsic star (point source)

Atmosphere and telescope cause a convolution

Detectors measure a pixelated image

Image also contains noise

The shape and size of images are affected by the PSF, which results from the telescope optics, bed focusing, etc. and for ground-based images, from atmospheric turbulence.

The PSF correction is the most difficult, yet most important step in the measurement of lensing signal.

COSMIC SHEAR MEASUREMENT

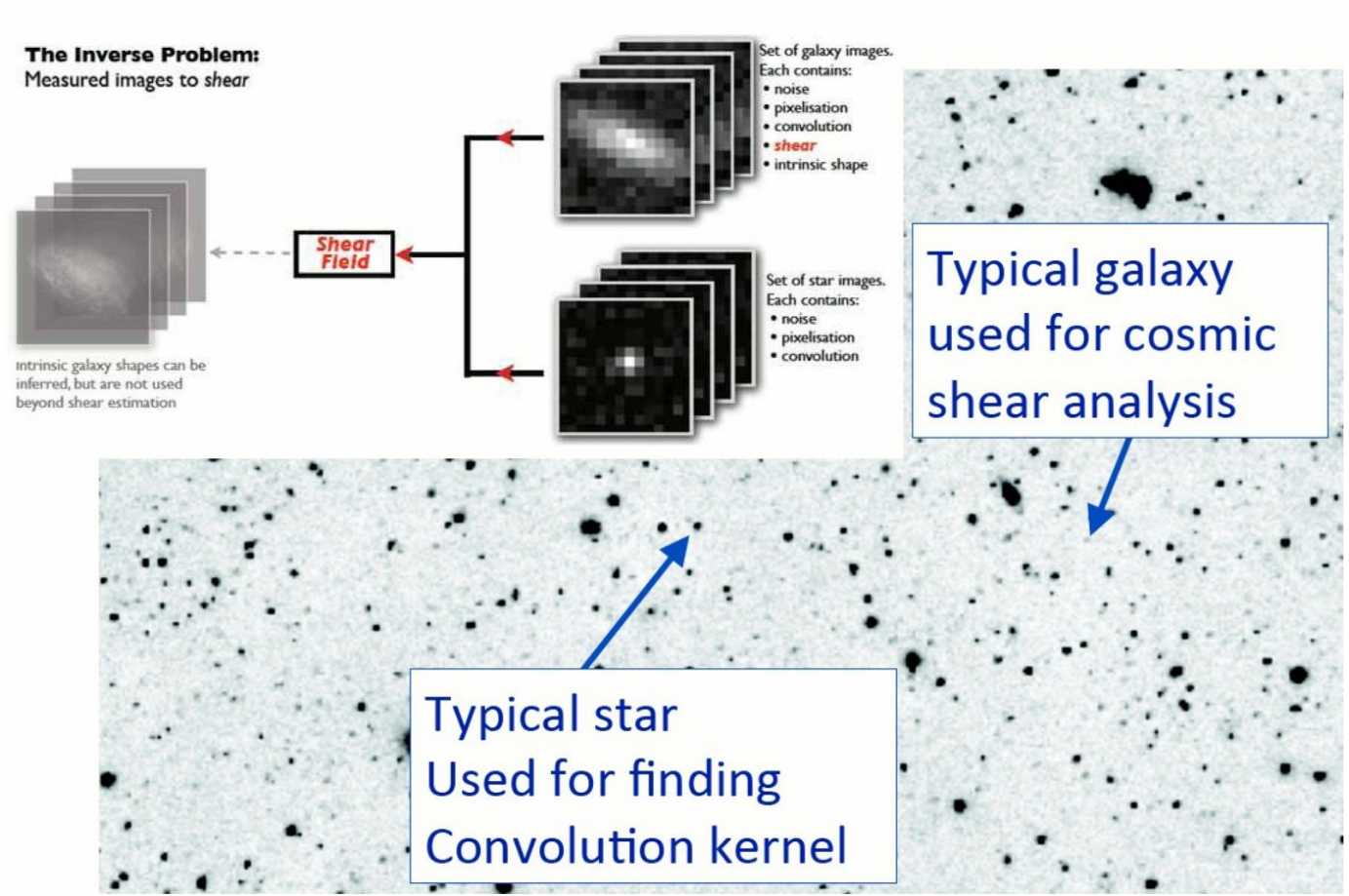

COSMIC SHEAR COSMOLOGY

Cosmic Shear:

- Map the matter distribution directly (no assumption about the relation between DM and baryonic matter)
- Lensing measurements are sensitive to the geometry and provide measures of the growth of LSS → powerful probe of DE and modified gravity theories
- It helps in breaking parameter degeneracies when combined with other cosmological probes

First detection of cosmic shear in 2000 by four independent groups (Bacon et al. 2000; Kaiser et al. 2000; van Waerbeke et al.; Wittman et al. 2000) using ~10^5 galaxies, 1 deg^2.
Current results from >10^8 galaxies over a few 10^3 deg^2.

Weak lensing mass map with redMaPPer clusters derived from DES Y3 shear catalogue of 100,204,026 galaxies in 4143 deg^2 .

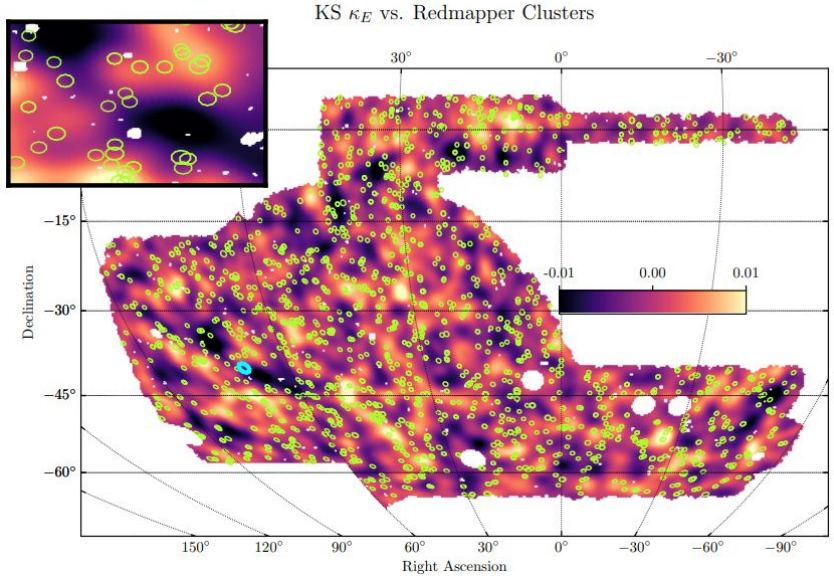

COSMIC SHEAR COSMOLOGY

Cosmic Shear:

- Map the matter distribution directly (no assumption about the relation between DM and baryonic matter)
- Lensing measurements are sensitive to the geometry and provide measures of the growth of LSS → powerful probe of DE and modified gravity theories
- It helps in breaking parameter degeneracies when combined with other cosmological probes

First detection of cosmic shear in 2000 by four independent groups (Bacon et al. 2000; Kaiser et al. 2000; van Waerbeke et al.; Wittman et al. 2000) using ~10^5 galaxies, 1 deg^2.
Current results from >10^8 galaxies over a few 10^3 deg^2.

DES Y3 + KIDS-1000 Shear result

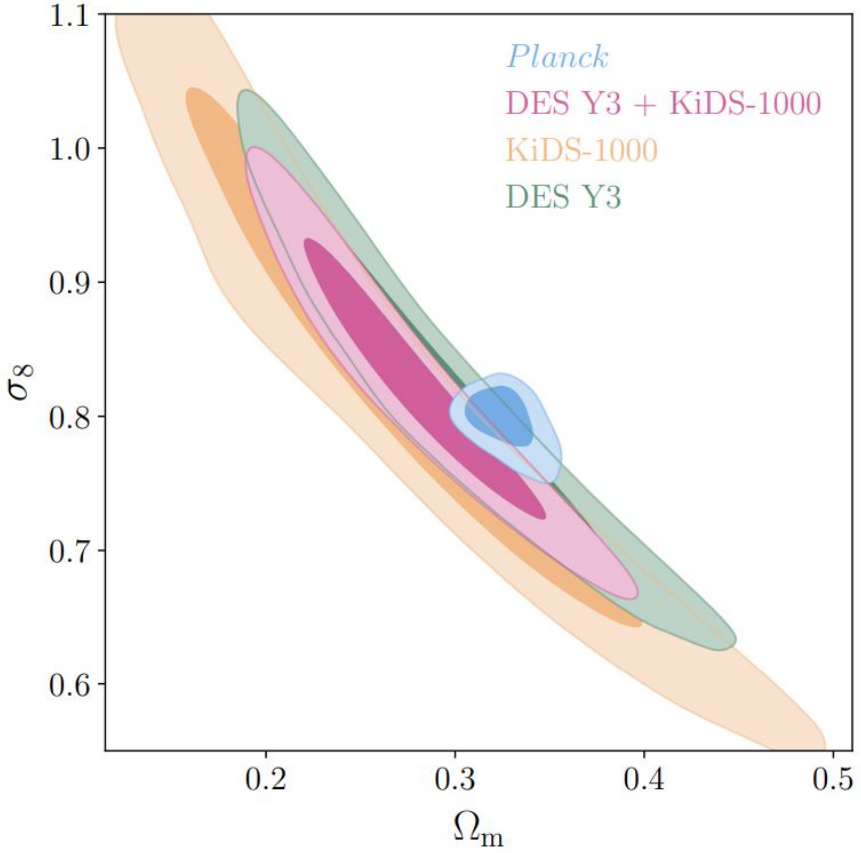

https://arxiv.org/pdf/2305.17173.pdf

CMB LENSING POWER SPECTRUM

CMB lensing effect leaves subtle imprints in the temperature and polarization anisotropies, which can be used to reconstruct a map of the lensing potential whose gradient determines the lensing deflections. For example, in propagating through a large overdense clump of matter on the line of sight, angular structures in the CMB get magnified appearing bigger on the sky. Essentially, by looking how the typical size of hot and cold spots in the CMB temperature map vary across the sky, we can reconstruct the lensing deflections and hence the integrated distribution of dark matter.

The lensing map provides a new cosmological observable, similar to maps of cosmic shear estimated from the shapes of galaxies. Its power spectrum (see below) provides access to cosmological parameters from the CMB alone that affect the late-time expansion and geometry of the Universe, and the growth of structure — parameters that have only degenerate effects in the primary CMB anisotropies.

The lensing map reconstructed from the Planck 2018 data

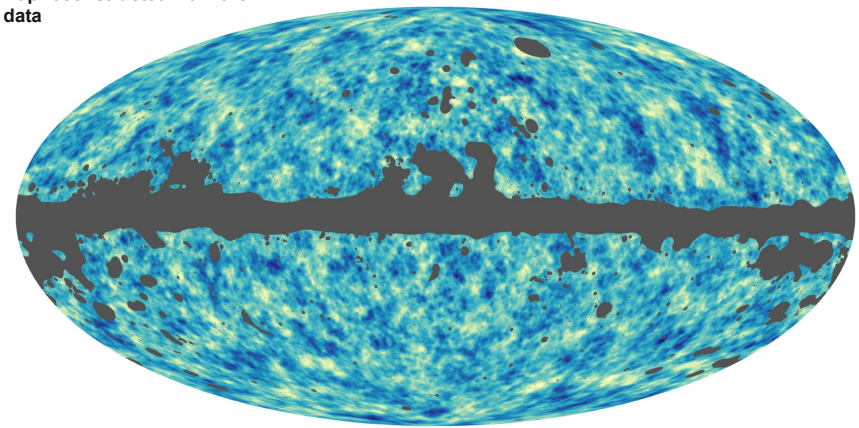

CMB LENSING POWER SPECTRUM

Lensing breaks the statistical **isotropy** of the CMB, introducing correlations between different scales (multipoles).

The lensed temperature T can be expressed in terms of the unlensed temperature T̃ shifted by a deflection angle $\alpha = \nabla \phi$

$$T(\hat{n}) = \tilde{T}(\hat{n} + \nabla\phi(\hat{n})) \approx \tilde{T}(\hat{n}) + \nabla\phi(\hat{n}) \cdot \nabla\tilde{T}(\hat{n})$$

The potential ϕ can be reconstructed by looking at the correlation between two different modes (l_1, l_2) in Fourier space. In an unlensed universe, these modes are independent. With lensing, they are mixed:

$$\langle T(\ell_1)T(\ell_2)\rangle_{\text{fixed }\phi} \approx f(\ell_1, \ell_2)\phi(\ell_1 + \ell_2)$$

f(l_1, l_2) is a weight function that maximizes the signal-to-noise ratio

The lensing map reconstructed from the Planck 2018 data

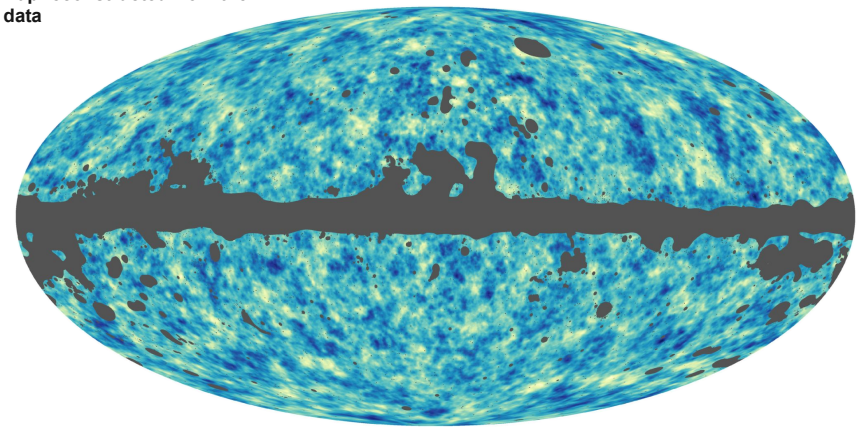

By measuring how the small-scale CMB fluctuations are spatially correlated with the large-scale CMB gradients, we can reconstruct the underlying gravitational potential ϕ that caused the distortion

CMB LENSING POWER SPECTRUM

The lensing potential is an integrated measure of all the matter (dark and baryonic) between us and the Surface of Last Scattering.

$$C_\ell^{\phi\phi} = \frac{4}{\ell^4}\int_0^{\chi_*} \frac{W^2(\chi)}{\chi^2} P_m(k,z)d\chi$$

- **Amplitude:** Tells us the total amount of matter in the universe and amplitude of fluctuatians (Ω_m, σ_8).
- **Shape:** Tells us how structure grew over time, which is also sensitive to total neutrino masses and Dark Energy.

Power spectrum of the CMB lensing potential estimated from the 4-point function (trispectrum) of the Planck 2018 temperature and polarization maps (pink boxes), compared with the theoretical expectation for the LCDM model with parameters determined from the Planck measurements of the CMB power spectra.

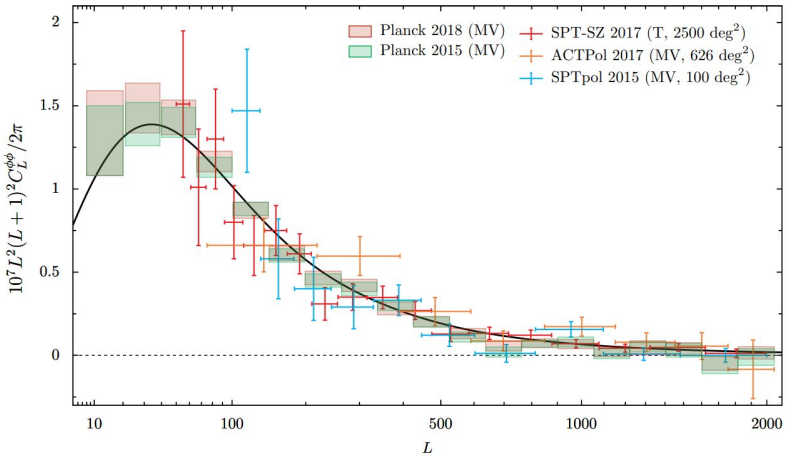

CMB LENSING POWER SPECTRUM

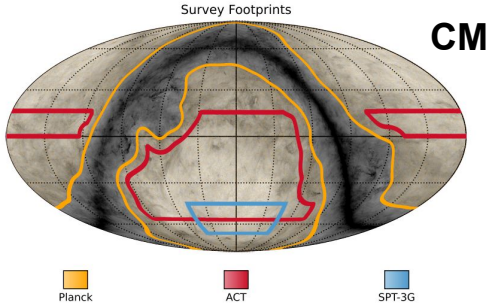

CMB lensing from Planck+ACT+SPT

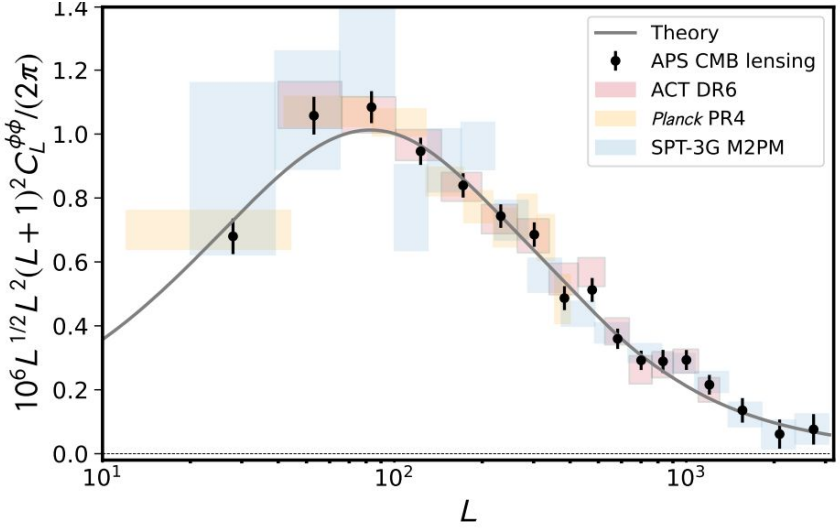

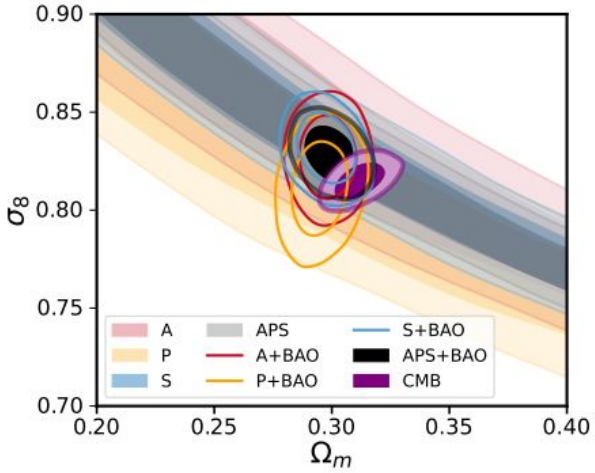

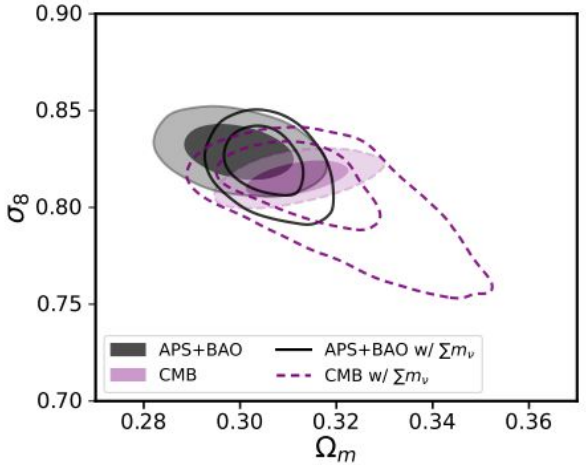

See: https://arxiv.org/pdf/2504.20038

STATISTICAL PROPERTIES OF THE LARGE SCALE STRUCTURES:

MULTI-PROBE COSMOLOGY

see e.g. https://lss.fnal.gov/archive/2013/pub/fermilab-pub-13-441-a.pdf
https://arxiv.org/pdf/1601.05779
https://arxiv.org/pdf/2105.13548

MULTI-PROBE COSMOLOGY AND CROSS-CORRELATION

In the last decade it becomes clear that combining different probes of the LSS could greatly improve the constraining power at the expense of a more complicated modeling. In particular, if we combine different tracers of the same matter density field, they will exhibit covariance (e.g. in an area where the density of galaxies is high at some redshift, the distortion of background objects by gravitational lensing will also be greater). We can measure the degree of covariance between a cosmological observable; these cross-correlation functions can provide information not given by each observable on its own.

Cross Angular Power Spectrum of two tracers *a* and *b* :

$$\langle a_{\ell m} b^*_{\ell m} \rangle \equiv C^{ab} \delta_{\ell \ell'} \delta_{m m'}$$

$$C_\ell^{ab} = 4\pi \int_0^\infty \frac{dk}{k} \mathcal{P}_\Phi(k) \Delta_\ell^a(k) \Delta_\ell^b(k)$$

Primordial matter power spectrum

Transfer functions of the tracers (e.g. galaxy, lensing, cluster)

MULTI-PROBE COSMOLOGY: 3x2pt

- **The combination of galaxy clustering, cosmic shear, and galaxy–galaxy lensing measurements – the so called 3x2pt analysis – has proven to provide powerful constraints on the structure formation in the late universe, while self calibrating many astrophysical (e.g. galaxy bias) or systematic parameters (e.g. intrinsic alignments and photo-z errors) in the model.**

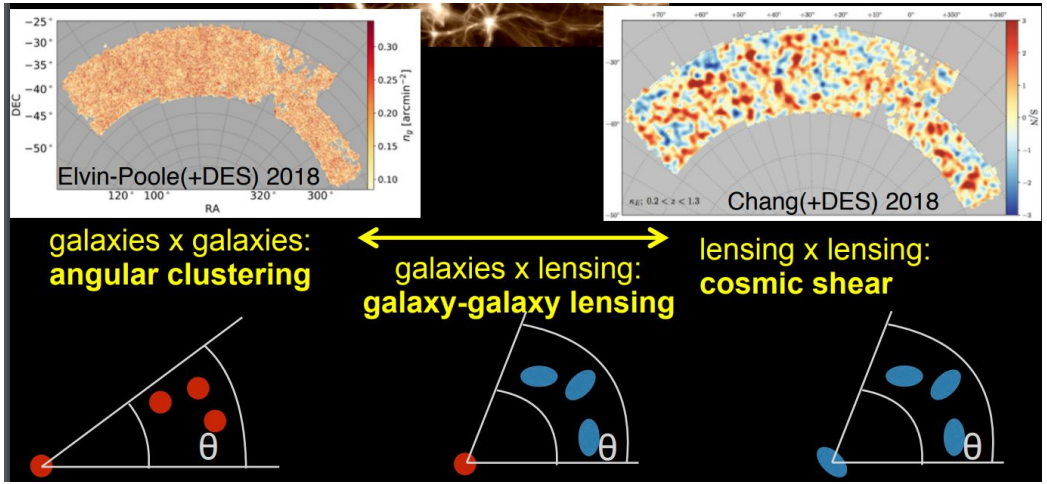

DES Y3 3x2pt analysis

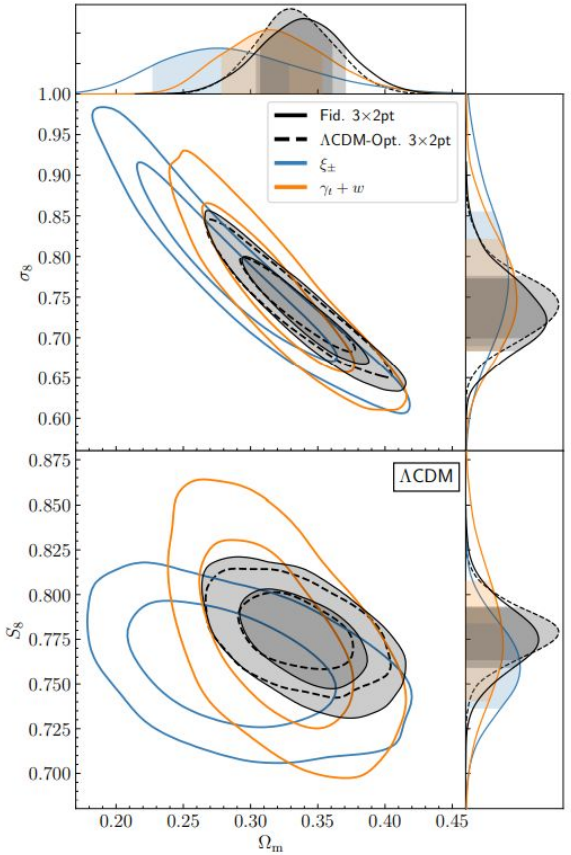

https://arxiv.org/pdf/2105.13549.pdf

MULTI-PROBE COSMOLOGY: DES Y1 6x2pt+N

- **The cosmological constraints can be further improved (at the expense of a more complicated model), by including galaxy clusters abundance and auto-cross correlation functions:**

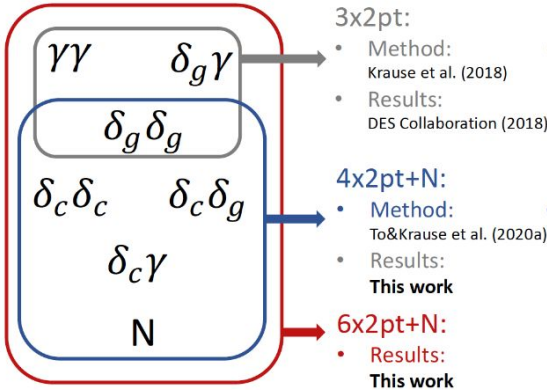

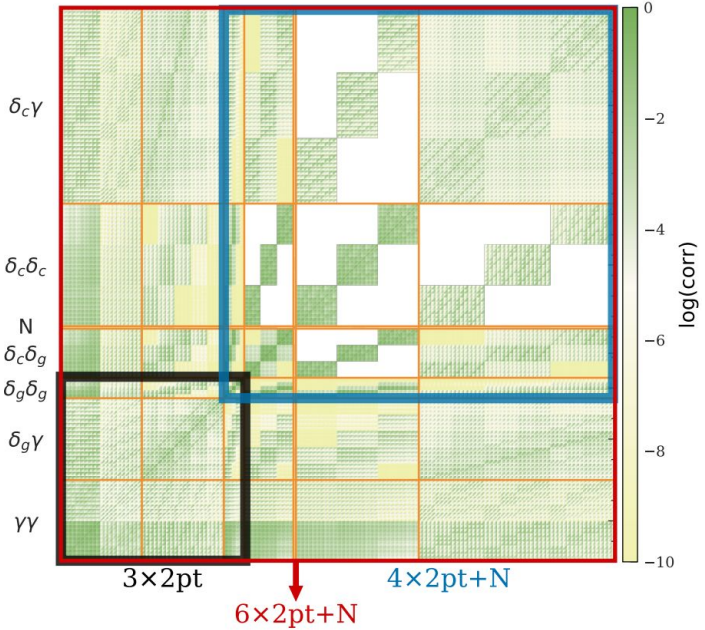

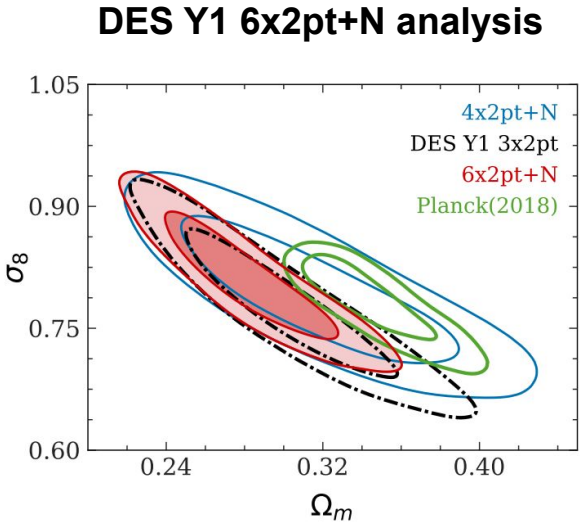

Correlation matrix for the combined analysis of galaxy, lensing and cluster correlation function and cluster counts

To et al 2021

MULTI-PROBE COSMOLOGY: DES Y3 6x2pt+N

- **The cosmological constraints can be further improved (at the expense of a more complicated model), by including galaxy clusters abundance and auto-cross correlation functions:**

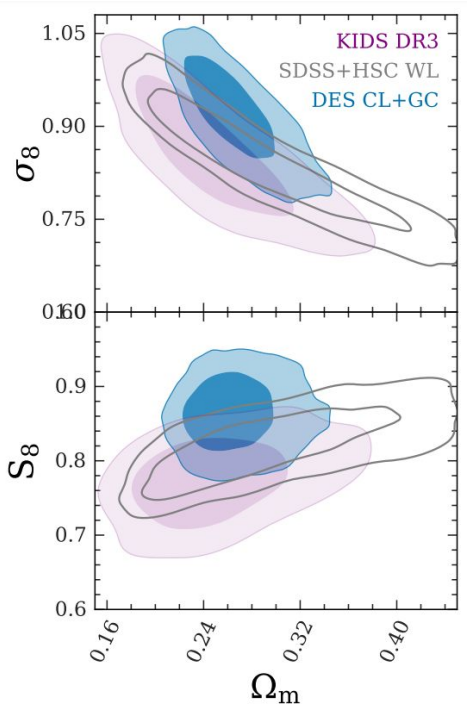

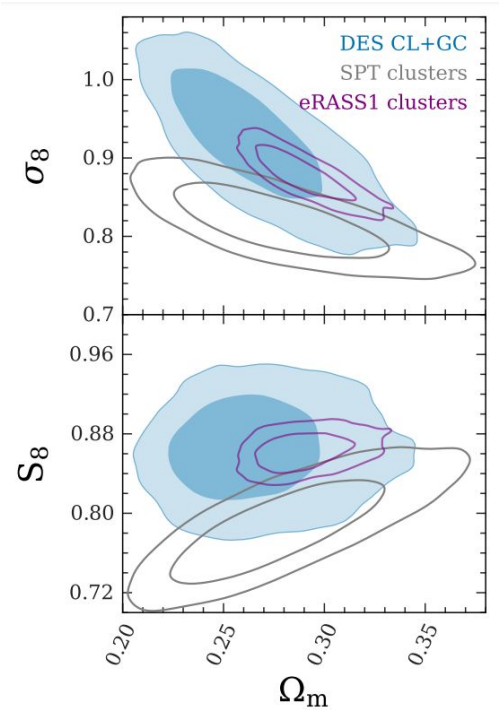

$$S_8 = 0.864 \pm 0.035$$

$$\Omega_m = 0.265^{+0.019}_{-0.031}$$

$$\sigma_8 = 0.922^{+0.063}_{-0.049}.$$

https://arxiv.org/abs/2503.13632

MULTI-PROBE COSMOLOGY: 3x2pt DES+N SPT

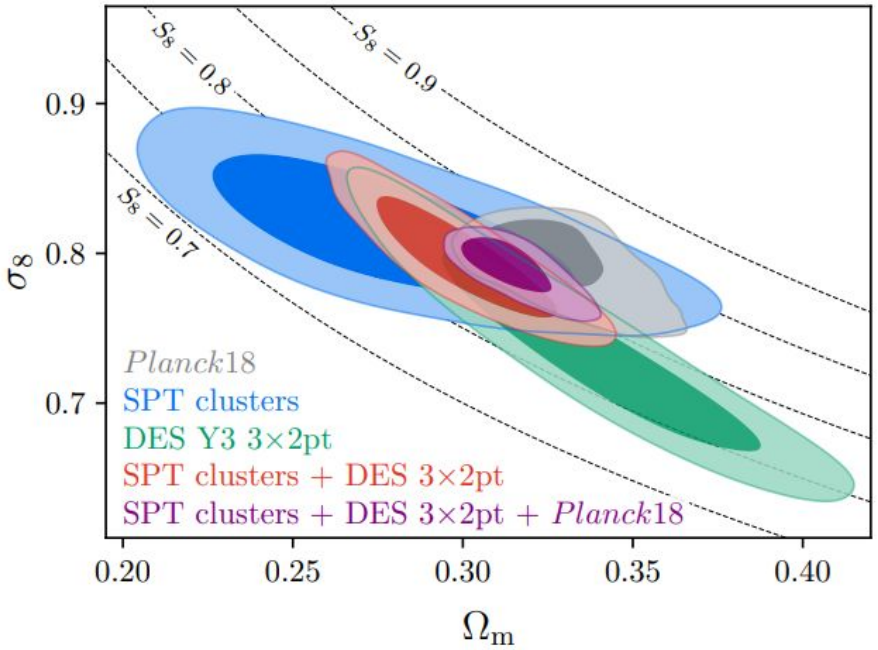

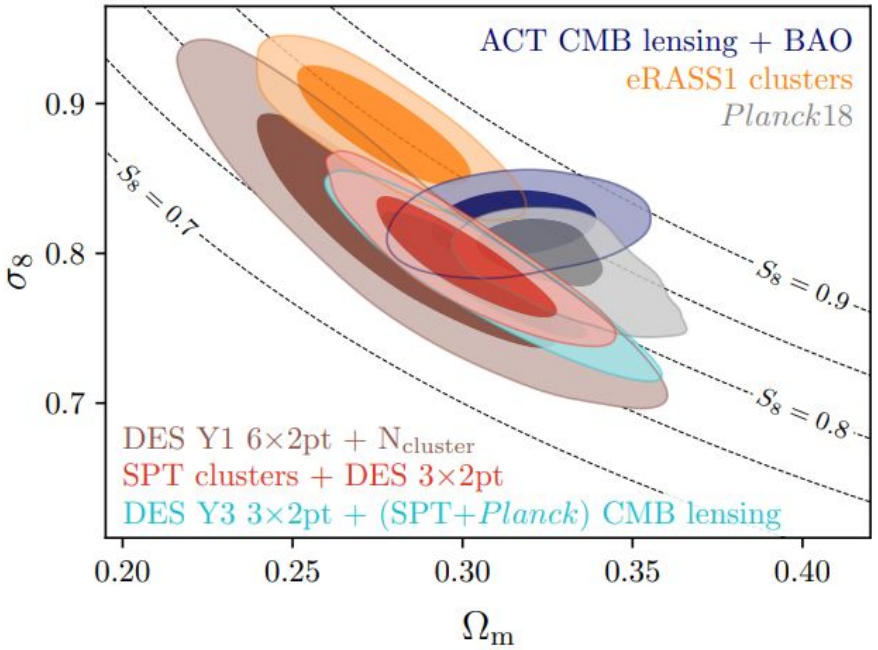

https://arxiv.org/abs/2412.07765